Interaction of photons traversing a slowly varying electromagnetic background: Numerical simulation of frequency cascading

H. Ruhl, B. King, P. Böhl, A. Domenech

Physics Department, LMU Munich, Germany
ELI-NP 2015, Bucharest

Sept. 21, 2015

LMU

Overview

- A framework for strong laser field physics.
- Numerical issues
- Benchmarks
- Strong fields
- The Heisenberg-Euler effective Lagrangian.
- Wave equations
- Numerical scheme
- Numerical results
- Frequency cascades

Basic parameters

Some basic scales of the system are

$$n_0\,, \quad A_0\,, \quad E_S = \frac{m^2 c^3}{e\hbar}\,, \quad \lambda\,, \quad \lambda_C = \frac{\hbar}{mc}\,, \quad t = \frac{\lambda}{c}\,, \quad t_C = \frac{\lambda_C}{c}\,. \tag{1}$$

The non-linearity parameters of the field are

$$a_0 = \frac{eA_0}{mc}\,, \quad \mathcal{F} = \frac{c^2\vec{B}^2 - \vec{E}^2}{2}\,, \quad \mathcal{G} = c\,\vec{E}\cdot\vec{B}\,. \tag{2}$$

The non-linearity parameters of the seeded processes of radiation and electron-positron pair production are

$$\chi_\pm = \frac{e\hbar}{m^3c^4}\sqrt{\left(\frac{\varepsilon_\pm\vec{E}}{c} + c\vec{p}_\pm\times\vec{B}\right)^2 - (\vec{p}_\pm\cdot\vec{E})^2}\,, \tag{3}$$

$$\chi_\gamma = \frac{e\hbar}{m^3c^4}\sqrt{\left(\frac{\varepsilon_\gamma\vec{E}}{c} + c\vec{k}\times\vec{B}\right)^2 - (\vec{k}\cdot\vec{E})^2}\,, \tag{4}$$

where p^- is the electron momentum, p^+ the positron momentm, and k the photon momentum.

Strong field effects in the a_0 and γ landscape

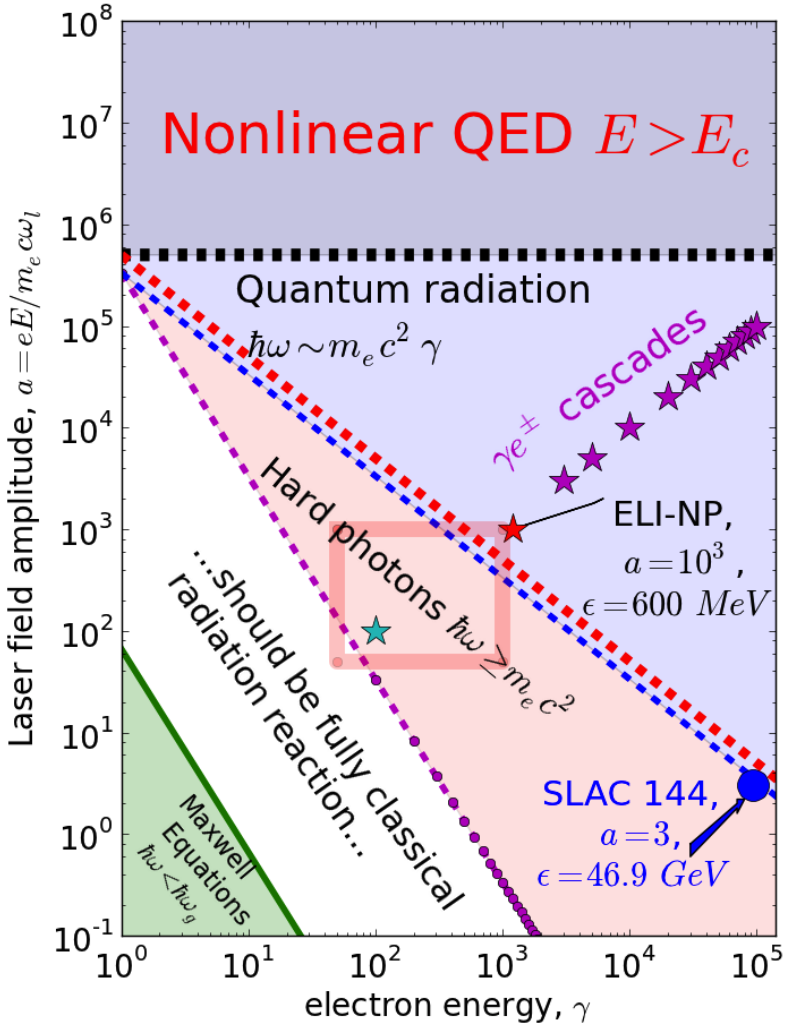

Classical radiating particle systems

The force equations for individual electrons consist of LAD and other electron contributions. They are given by

$$m\,\frac{du_i^\mu}{d\tau_i} = \frac{e}{c}\,F_i^{\mu\nu}(x_i^\rho)\,u_{\nu i} + m\,\tau_0\,\Delta^{\mu\nu}(u_i^\rho)\,\frac{d\gamma_{\nu i}}{d\tau_i}\ ,$$

$$\Delta^{\mu\nu}(u^\rho) = g^{\mu\nu} - \frac{u^\mu u^\nu}{c^2}\ ,\quad \gamma_{\nu i} = \frac{du_{\nu i}}{d\tau_i}\ ,\quad \tau_0 = \frac{2e^2}{3mc^3}\ .$$

The equations above have to be augumented with expressions for retarded em fields for point electrons. In mean field approximation an extended Vlasov equation containing radiation is obtained (see Hakim et al. 1968)

$$\begin{aligned}
&\partial_\tau R^1\left(X^\rho,\tau\right) + u^\mu\,\partial_\mu^x R^1\left(X^\rho,\tau\right)\\
&+\frac{4\pi e^2}{mc^2}\,u_\nu\int d\tau'\,d^4x'\,d^4u'\left(u^{\mu\prime}\,\partial^{x\nu} - u^{\nu\prime}\,\partial^{x\mu}\right)D_{ret}\left(x^\rho - x^{\rho\prime}\right)R^1\left(X^{\rho\prime},\tau'\right)\partial_\mu^u R^1\left(X^\rho,\tau\right)\\
&= -\tau_0\,\partial_\mu^u\left[\Delta^{\mu\nu}(u_\rho)\int d^4\dot\gamma\,\dot\gamma_\nu\,f^1\left(X^\rho,\dot\gamma^\rho,\tau\right)\right]\ ,
\end{aligned}$$

where $X = (x, u)$ and

$$R^1\left(X^\rho,\tau\right) = \int d^4\dot\gamma\,f^1\left(X^\rho,\dot\gamma^\rho,\tau\right)\ .$$

The radiation field is stored in the electrons and the retarded Greens function D_{ret}. The red force above is the mean field force, which is solved numerically with the help of Maxwell's equations. The blue force is the LAD force.

Kinetic equations for e^-, e^+ and γ

- Each phase space volume element for electrons and positrons has gains and losses. The corresponding rate equations are (see relativistic quantum kinetic equations, lecture course by H. Ruhl, LMU, Munich)

$$\left(\partial_t + \vec{v}\cdot\partial_{\vec{x}} + \vec{F}\cdot\partial_{\vec{p}}\right) f_\pm(\vec{x},\vec{p},t) \tag{5}$$
$$= \int d^3k\, \frac{dW_\gamma}{d^3k}(\vec{k},\vec{p}+\vec{k})\, f_\pm(\vec{x},\vec{p}+\vec{k},t) - f_\pm(\vec{x},\vec{p},t) \int d^3k\, \frac{dW_\gamma}{d^3k}(\vec{k},\vec{p})$$
$$+ \int d^3k\, \frac{dW_\pm}{d^3p}(\vec{k},\vec{p})\, f_\gamma(\vec{x},\vec{k},t) + S(\vec{x},\vec{p},t)\ .$$

- Radiation is modeled with the help of coherent fields and incoherent photons. Each phase space element for photons has gains and losses. The corresponding balance is

$$\left(\partial_t + \frac{c^2\,\vec{k}}{\omega}\cdot\partial_{\vec{x}}\right) f_\gamma(\vec{x},\vec{k},t) \tag{6}$$
$$= \int d^3p\, \frac{dW_\gamma}{d^3k}(\vec{k},\vec{p})\ \left[f_+(\vec{x},\vec{p},t) + f_-(\vec{x},\vec{p},t)\right]$$
$$- f_\gamma(\vec{x},\vec{k},t) \int d^3p\, \frac{dW_\pm}{d^3p}(\vec{k},\vec{p})\ .$$

The coherent fields are modeled with the help of nonlinear Maxwell equations.

Spontaneous vacuum decay

For a purely electric field the dissipative part of the Heisenberg-Euler Lagrangian can be approximated by (see related literature for the Wigner representation of the classical Dirac equation, lecture course H. Ruhl, LMU, Munich, lecture course H. Ruhl, LMU, Munich)

$$S(\vec{x},\vec{p},t) = \frac{1}{8\pi^3}\,\frac{E(\vec{x},t)}{m^2c^2\lambda_C^3 t_C E_S}\, e^{-\pi\, c\, \frac{m^2c^2+\vec{p}_\perp^{\,2}}{e\hbar E(\vec{x},t)}}\,\delta(p_\parallel)\,. \tag{7}$$

The total spontaneous pair production rate is (Schwinger formula)

$$\begin{aligned}\frac{dN_\pm}{dt} &= \int d^3x \int d\Omega \int dp_\parallel \int dp_\perp\, p_\perp\, S(\vec{x},\vec{p},t) \qquad (8)\\ &= \frac{1}{8\pi^3}\int d^3x \int d\Omega \int dp_\parallel \int dp_\perp\, p_\perp\, \frac{E(\vec{x},t)}{m^2c^2\lambda_C^3 t_C E_S}\, e^{-\pi c\,\frac{m^2c^2+\vec{p}_\perp^{\,2}}{e\hbar E}}\,\delta(p_\parallel)\\ &= \frac{1}{4\pi^3}\,\frac{V}{\lambda_C^3}\,\frac{E^2(\vec{x},t)}{E_S^2}\,\frac{1}{t_C}\, e^{-\pi\,\frac{E_S}{E}}\,.\end{aligned}$$

The Schwinger formula can be extended into the more general formula

$$\frac{dN_\pm}{dt} = \frac{1}{4\pi^3}\,\frac{V_{cell}}{\lambda_C^3}\,\frac{a\,b}{E_S^2}\,\coth\frac{b}{a}\,\frac{1}{t_C}\, e^{-\pi\,\frac{E_S}{a}}\,, \tag{9}$$

$$a = \sqrt{\sqrt{\mathcal{F}^2+\mathcal{G}^2}-\mathcal{F}}\,,\quad b = \sqrt{\sqrt{\mathcal{F}^2+\mathcal{G}^2}+\mathcal{F}}\,. \tag{10}$$

F. V. Bunkin and I. I. Tugov, Sov. Phys. Dokl. 14, 678 (1970). See discussion of the Heisenberg-Euler model.

Photon emission in constant-crossed fields

The probability rate for photon emission by an electron in a constant-crossed electromagnetic field is given by (see Ritus, Baier, and the textbook of Landau & Lifshitz for derivation, lecture course H. Ruhl, LMU, Munich)

$$\frac{dW_\gamma(\varepsilon_\gamma)}{d\varepsilon_\gamma} = -\frac{\alpha m^2 c^4}{\hbar \varepsilon_\pm^2}\left\{\int_x^\infty \mathrm{Ai}\,(\xi)\,d\xi + \left(\frac{2}{x}+\chi_\gamma\sqrt{x}\right)\mathrm{Ai}'(x)\right\}, \tag{11}$$

$$\int d\Omega\, k^2\,\frac{dW_\gamma}{d^3k} = \hbar c\,\frac{dW_\gamma}{d\epsilon_\gamma}, \quad \vec{p}_\pm(t+\delta t) = \vec{p}_\pm(t) - \vec{k}(t), \quad \vec{p}_\pm \parallel \vec{k}.$$

The parameter x is given by $x = \left(\chi_\gamma/\chi_\pm(\chi_\pm - \chi_\gamma)\right)^{(2/3)}$ with $0 \le \chi_\gamma < \chi_\pm$, Ai is the Airy function, ε_γ, and $\varepsilon_\pm$ are the energies of the photon, positron and electron, respectively. The quantum efficiency parameters $\chi_\pm$ and χ_γ are given on a previous slide.

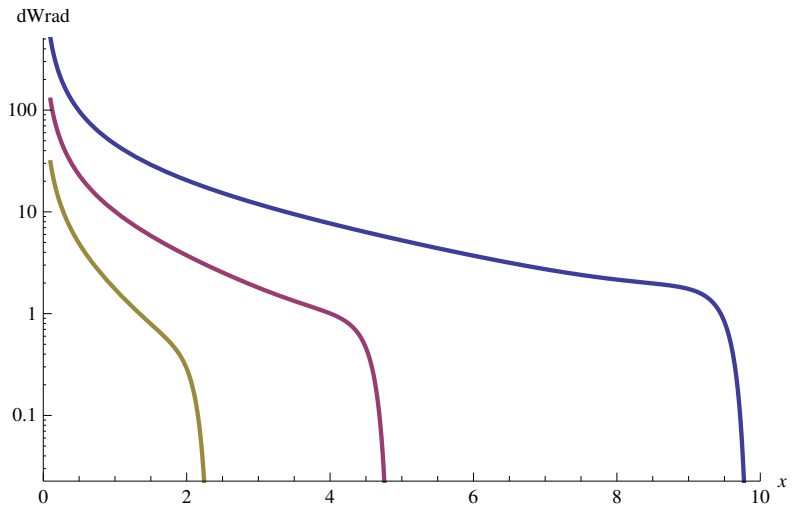

Pair creation in constant-crossed fields

The probability rate for pair creation by photons in a constant-crossed electromagnetic field is given by (see Fedotov, Ritus, Baier, and the textbook of Landau & Lifshitz for derivation)

$$\frac{dW_{\pm}(\varepsilon_{\pm})}{d\varepsilon_{\pm}} = \frac{\alpha m^2 c^4}{\hbar \varepsilon_{\gamma}^2} \left\{ \int_y^{\infty} \mathrm{Ai}\,(\xi)\, d\xi + \left(\frac{2}{y} - \chi_{\gamma} \sqrt{y} \right) \mathrm{Ai}'(y) \right\} , \tag{12}$$

$$\int d\Omega\, p_{\pm}^2 \, \frac{dW_{\pm}}{d^3 p_{\pm}} = \hbar c \, \frac{dW_{\pm}}{d\epsilon_{\pm}} , \quad \vec{p}_{+}(t+\delta t) + \vec{p}_{-}(t+\delta t) = \vec{k}(t) , \quad \vec{p}_{\pm} \parallel \vec{k} .$$

The parameter y is given by $y = \left(\chi_{\gamma}/\chi_{\pm}(\chi_{\gamma} - \chi_{\pm})\right)^{(2/3)}$ with $0 \leq \chi_{\pm} < \chi_{\gamma}$. The quantum efficiency parameters $\chi_{\pm}$ and χ_{γ} are given on a previous slide.

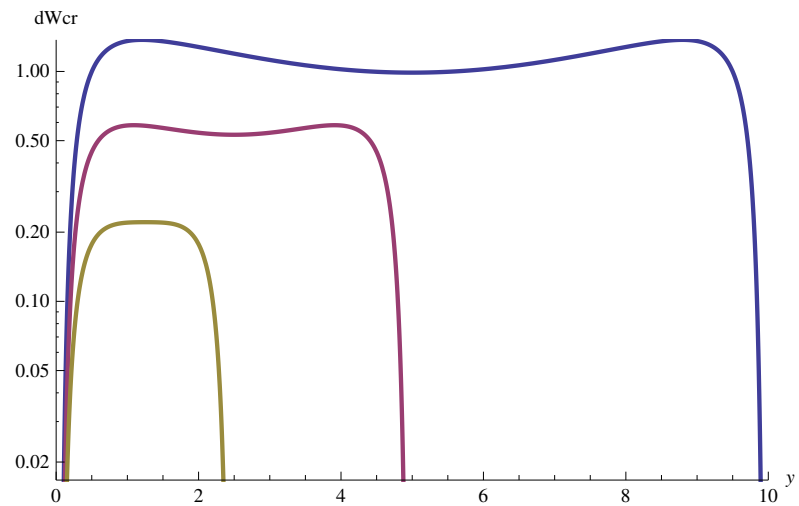

The numerical multi-scale problem

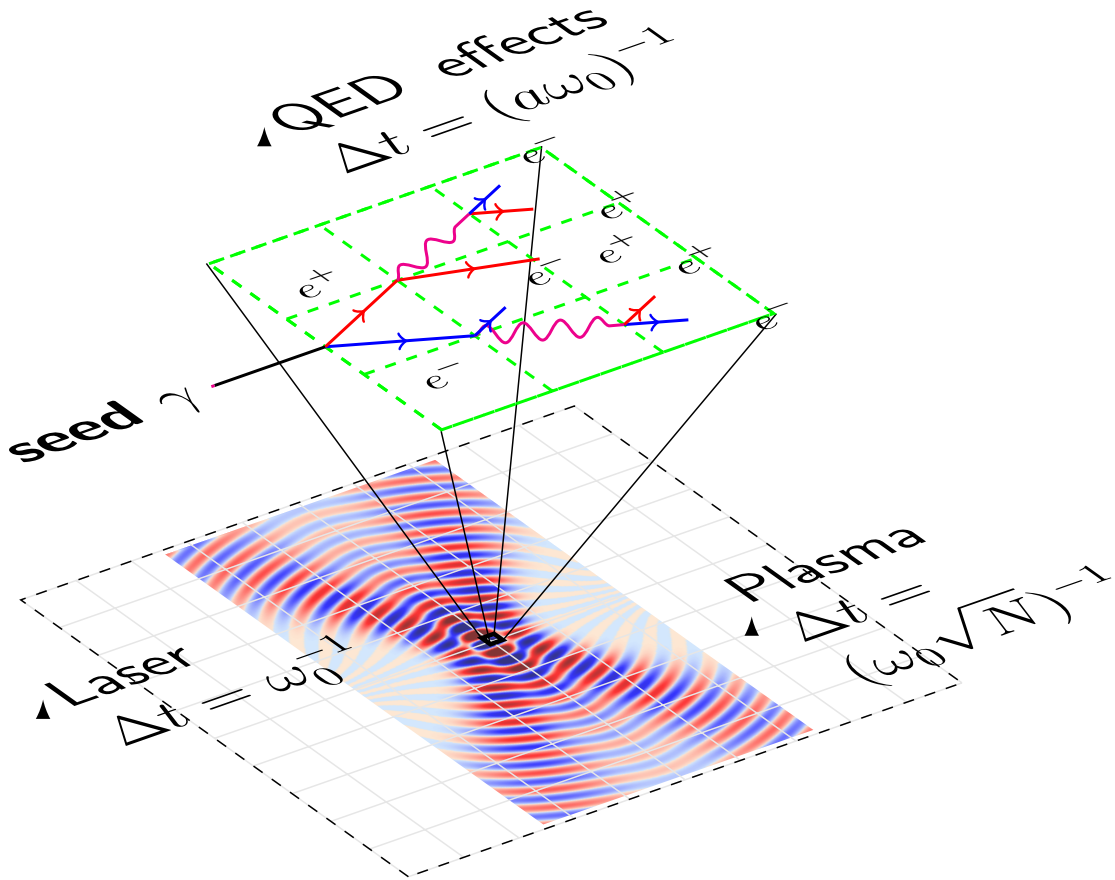

Adaptive particle load $\rightarrow$ APR-PIC

- Adaptive weights
$$f = \sum_i w_i \delta(\vec{u} - \vec{u}_i) S(\vec{r} - \vec{r}_i)$$
- Mass conservation
$$W = \sum w_i \rightarrow w_{1,2} = W/2$$
- Momentum conservation
$$\vec{P} = \sum_i \vec{u} w_i \rightarrow \vec{p}_{1,2} = \vec{P}/2 \pm \vec{Q}, \;\; \vec{Q} = |Q| \begin{pmatrix} -P_y \\ P_x \end{pmatrix}$$
- Energy conservation
$$\varepsilon = \sum_i w_i \sqrt{1 + \vec{u}_i}, \;\; |\vec{Q}| = 0.5 \sqrt{\varepsilon^2 - P^2 - W^2}$$

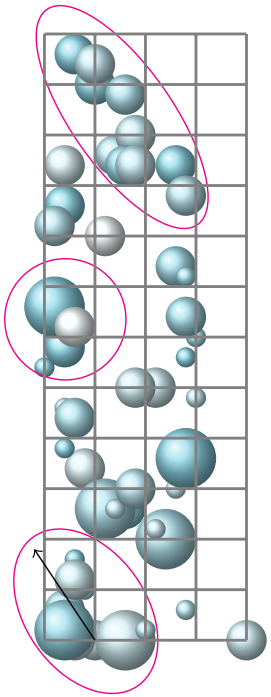

In addition, no divergence and currents must be generated during re-sampling.

N. Moschüring and H. Ruhl, Divergence free APR, in preparation.

Configuration space adaptivity → The AMR method

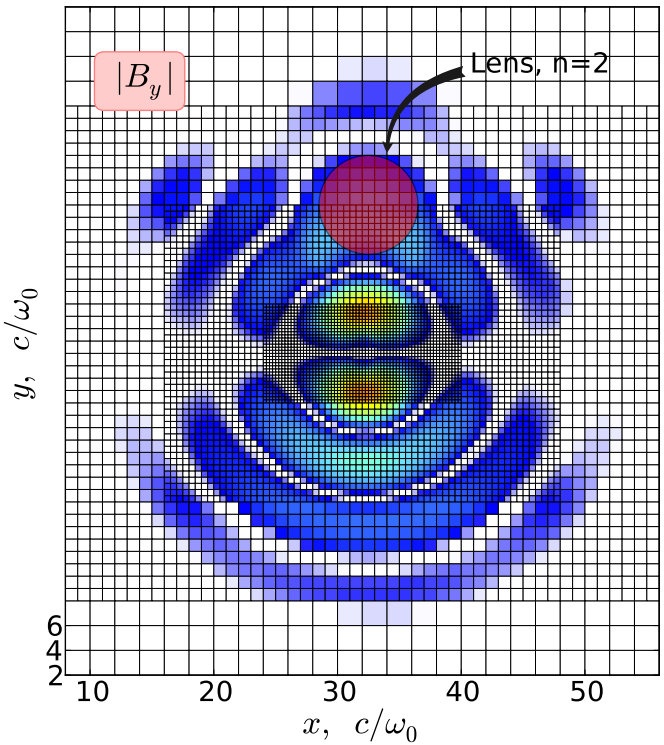

The plot shows a non-uniform grid with four resolution levels. There is a radiation source in the middle. The radiation passes through a lense. There is no reflection at the grid resolution boundaries. Grid adaptivity is presently not used in the PSC but will be employed for a future restart facility of the code.

N. Elkina and H. Ruhl, *An adaptive mesh refinement method for computational electromagnetics*, in preparation.

Weak and strong scaling behavior of the code

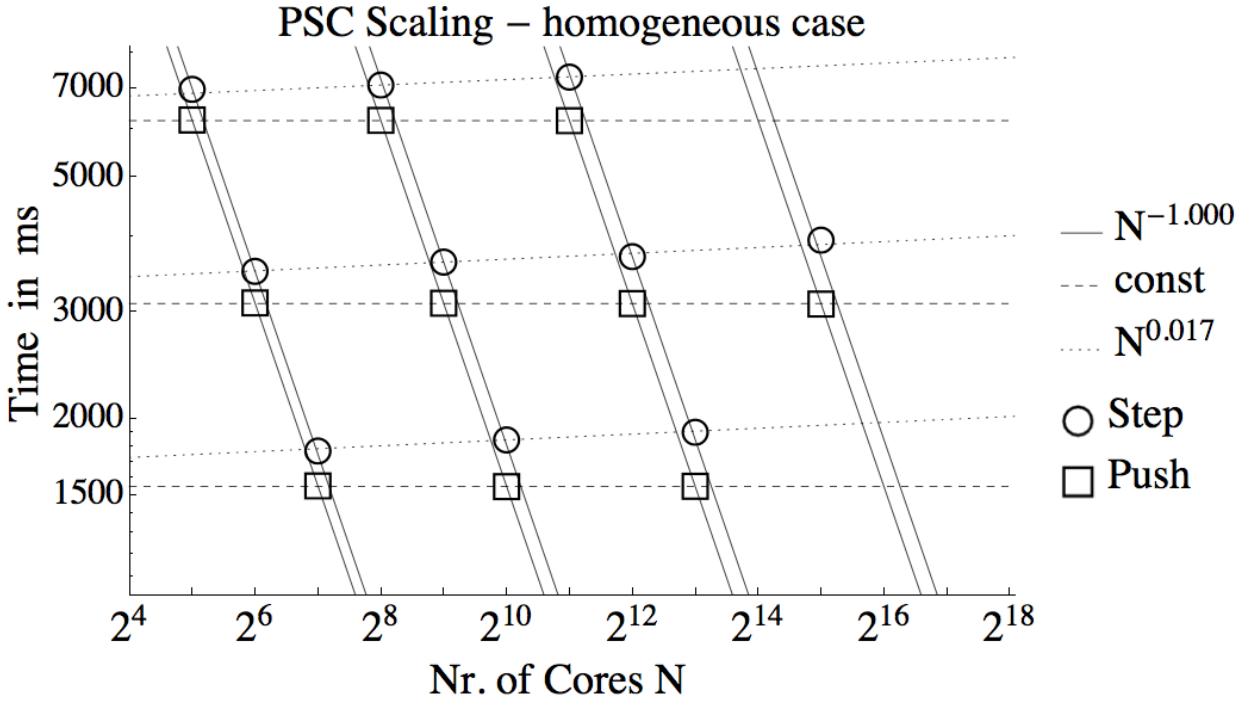

The plot shows the strong and weak scaling behavior of the PSC. The particle push operation and full integration steps are distinguished. For tests of weak scaling the problem size increases 8-fold for 8-fold the number of nodes. For strong scaling tests the problem size is fixed. Now, doubling the node number cuts the simulation time by half.

K. U. Bamberg and H. Ruhl, *Extreme Scaling of the PSC on SuperMUC at the LRZ*, inSiDE 12, 51 (2014).

The analytical solution of a 1D nano foil hit by a laser

A slowly varying envelope approximation has been applied!

$$\frac{dp_{xe}}{dt} = -\frac{\alpha}{2}\, sign(x_e) + \frac{a_0^2}{\gamma_e}\left(\sqrt{RT} + \frac{\alpha}{2}\,\frac{1}{\gamma_e\,(1+\beta_e)}\,T\right), \tag{13}$$

$$\frac{dx_e}{dt} = \frac{p_{xe}}{\gamma_e}, \tag{14}$$

$$R = 1 - T, \quad T = \frac{a^2}{a_0^2}, \quad \gamma_e = \gamma_{xe}\sqrt{1+a^2}, \quad \beta_e = \frac{p_{xe}}{\gamma_e}, \tag{15}$$

$$a = \sqrt{\frac{\sqrt{\left(1+\frac{1}{4}\alpha^2\gamma_{xe}^2\,(1+\beta_{xe})^2 - a_0^2\right)^2 + 4a_0^2} - \left(1+\frac{1}{4}\alpha^2\gamma_{xe}^2\,(1+\beta_{xe})^2 - a_0^2\right)}{2}}, \tag{16}$$

$$\psi = \arccos\frac{a}{a_0}, \tag{17}$$

$$a_0 = C\,\exp\left[-\frac{1}{2}\left(\frac{(t-t_{off})-x_e}{w}\right)^2\right], \tag{18}$$

$$C = 13{,}15{,}22 \quad \alpha = 8\pi, \quad x_e(0) = 0, \quad p_e(0) = 0, \quad t_{off} = 4\,w/c, \quad w = 1.5\lambda. \tag{19}$$

Analytical results at $a = 13$

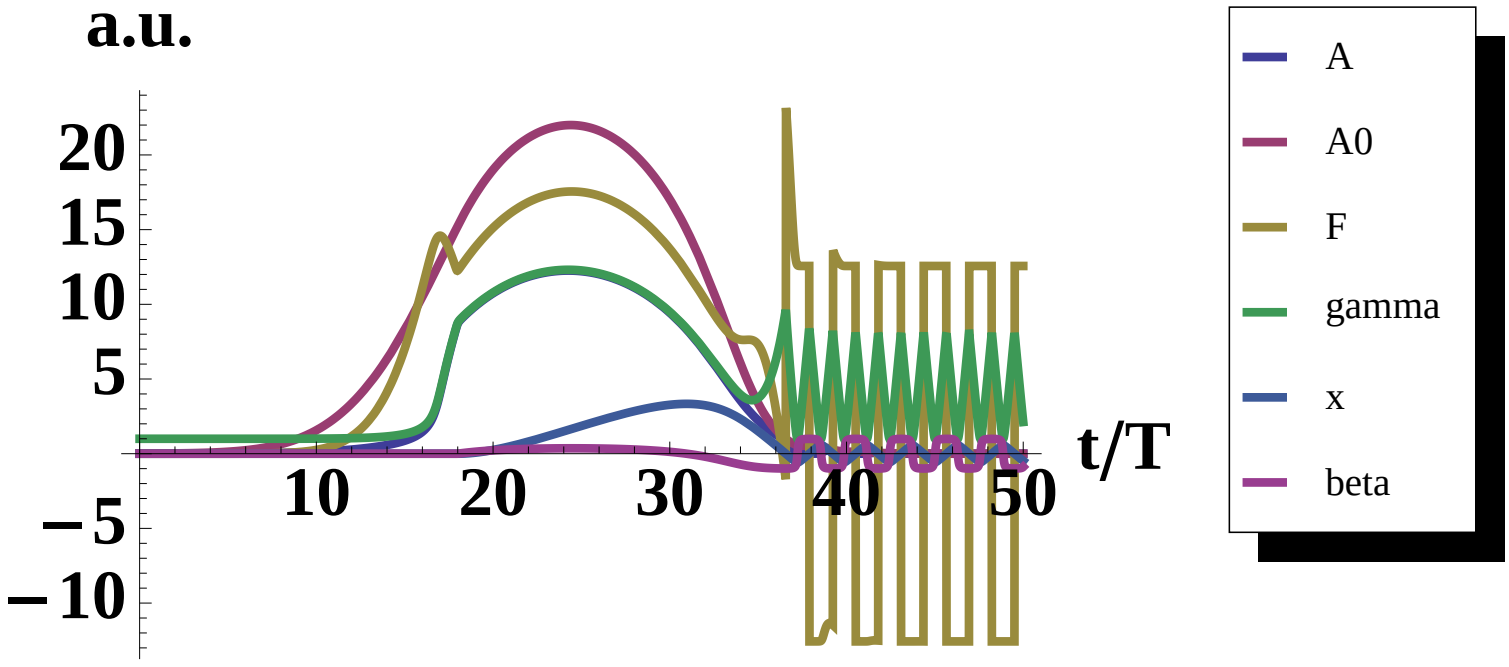

Numerical vs analytical at $a = 16$

Agreement is within expectation!

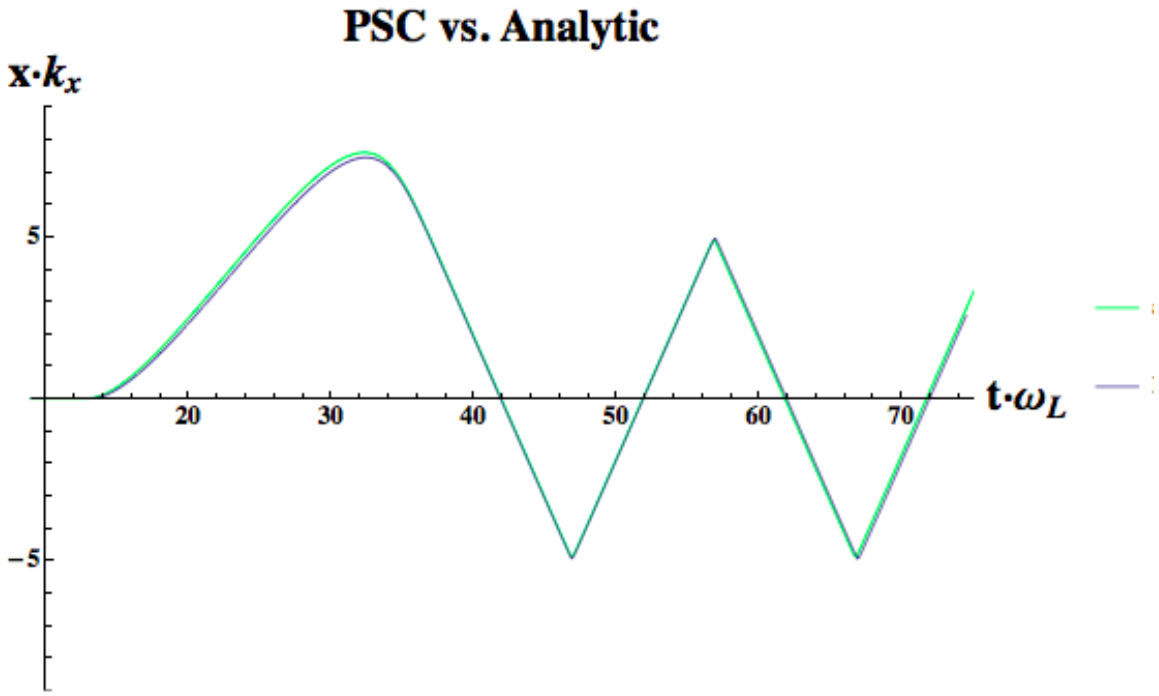

Green is analytic and grey is numerical data.

Quantum radiation from an e^- in a constant magnetic field

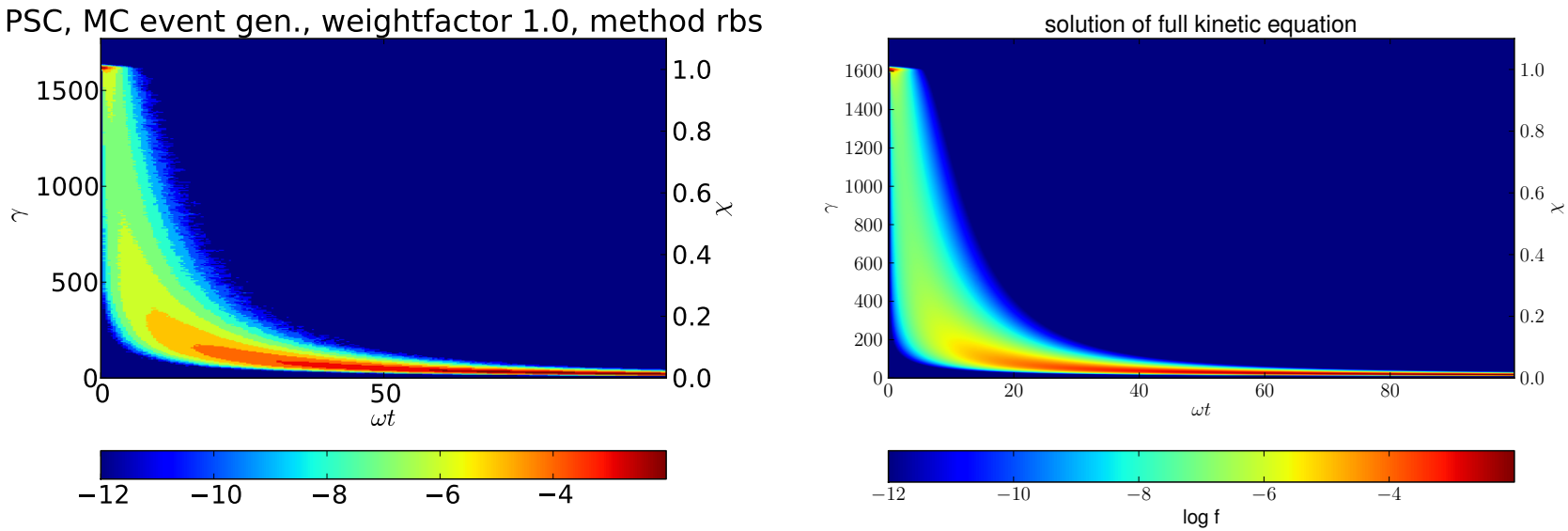

By courtesy of C. Klier. The plot shows the average energy γ versus time. Simulated data (left) and analytical data (right).

Constant rotating field: Growth of $N_{e^+e^-}$

$N(t) \sim e^{\Gamma t}$

$\Gamma \sim 1/t_{em} \sim \alpha \mu^{1/4} \sqrt{mc^2\omega/\hbar}$

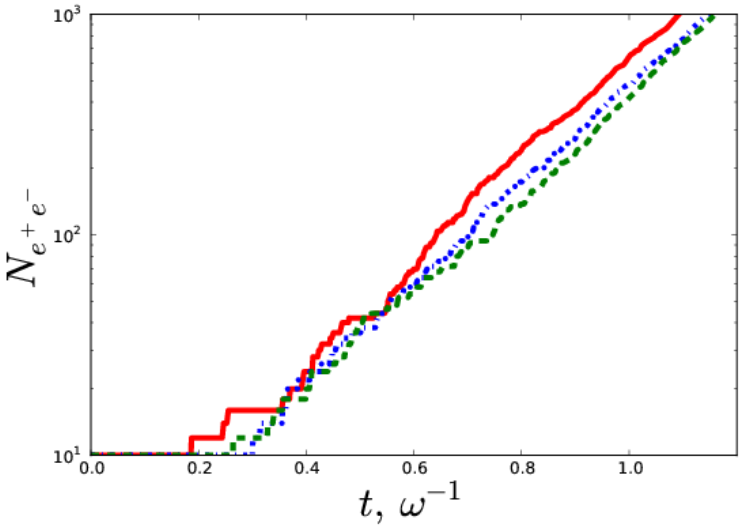

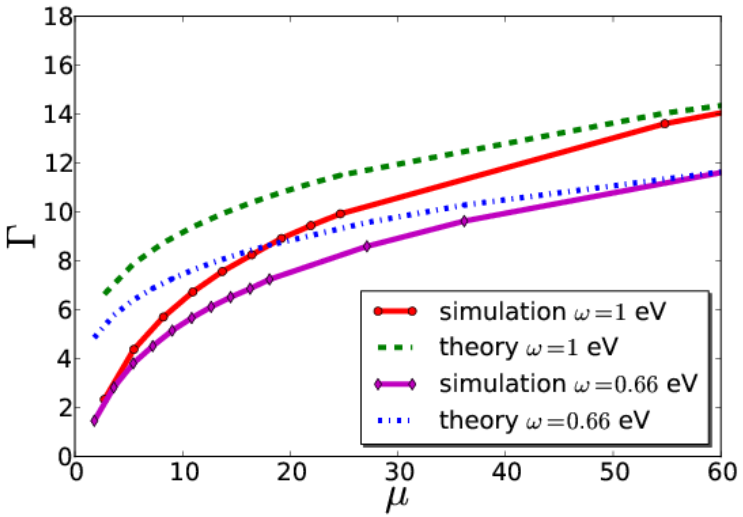

The number of pairs $N_{e^+e^-}$ as a function of time (results of three MC simulations for $a_0 = 2 \times 10^4$, $\omega = 1\,\text{eV}$, $\Gamma = 4.91 \pm 0.75$).

Parametric study of the growth rate $\Gamma(\mu)$ for pairs in the range between $a = (10 - 100) \times 10^4$, for $\omega = 1\,eV$, and $\omega = 0.66\,eV$.

Elkina N., Fedotov A. M., Kostyukov I. Yu., Legov M. V., Narozhny N. B., Nerush E. N. , and **Ruhl H.**, *QED cascades induced by circularly polarized laser fields*, Phys. Rev. ST. Accel. **14**, 054401 (2011).

Radiation friction

$$\frac{d\vec{p}_i}{dt} = -e\left(\vec{E} + \vec{v}_i \times \vec{B}\right) - \frac{\vec{p}}{|\vec{p}|}\int d^3k\ \vec{k}\ \frac{dW_{rad}}{d^3k}\left(\vec{p}_i, \vec{k}\right)\ , \tag{20}$$

$$\begin{aligned}\vec{E}(\vec{x}, t) = E_0\, e^{-\frac{l^2}{2d^2}(x^2+y^2)} \Bigg(& e^{-\frac{2\pi}{\Delta\phi^2}(t-z)^2} \cos\left[2\pi(t-z)\right] \\ & + e^{-\frac{2\pi}{\Delta\phi^2}(t+z)^2} \cos\left[2\pi(t+z)\right] \Bigg)\ \vec{e}_x \\ & + E_0\, e^{-\frac{l^2}{2d^2}(x^2+y^2)} \Bigg(e^{-\frac{2\pi}{\Delta\phi^2}(t-z)^2} \sin\left[2\pi(t-z)\right] \\ & + e^{-\frac{2\pi}{\Delta\phi^2}(t+z)^2} \sin\left[2\pi(t+z)\right] \Bigg)\ \vec{e}_y\ ,\end{aligned} \tag{21}$$

$$\partial_t \vec{B}(\vec{x}, t) = -\vec{\nabla} \times \vec{E}(\vec{x}, t)\ . \tag{22}$$

Radiation friction: PSC simulation

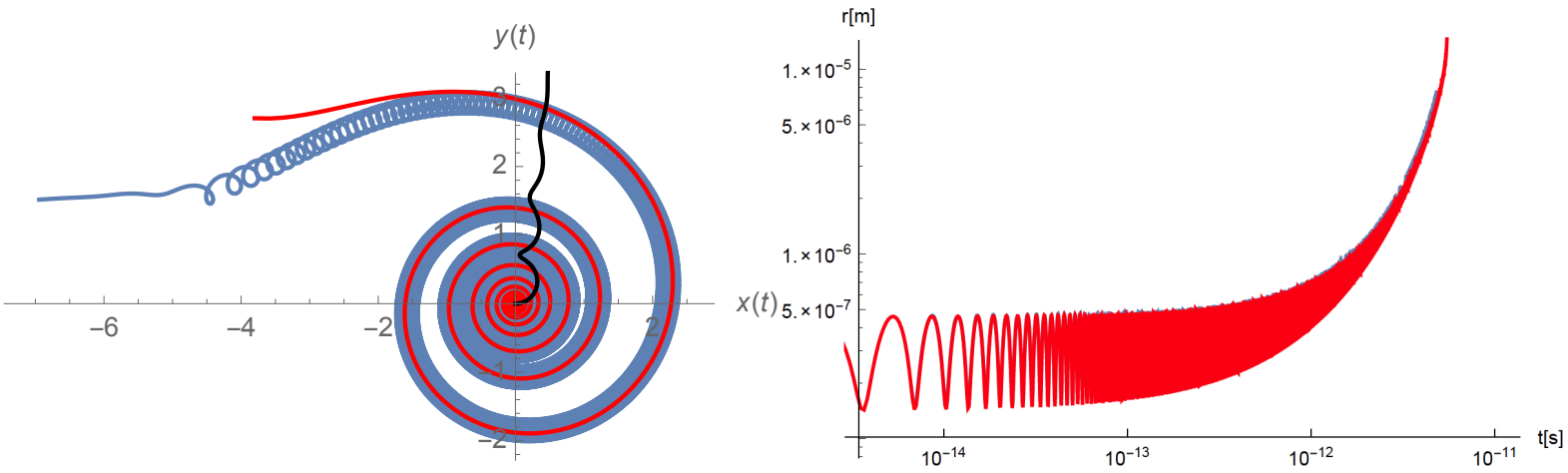

Plot (a) shows the guiding center motion of a single radiating electron in the rotating electromagnetic field for $a_0 = 800$. The electron is trapped in the high field region for a long time as can be concluded from plot (b), which gives the radius r of the electrons measured from the center for the external field as a function of time. Without radiation friction the electron would drift away quickly.

A. M. Fedotov, N. V. Elkina, E. G. Gelfert, N. B. Narozhny, H. Ruhl, PRE (2015).

Radiation friction: PSC simulation

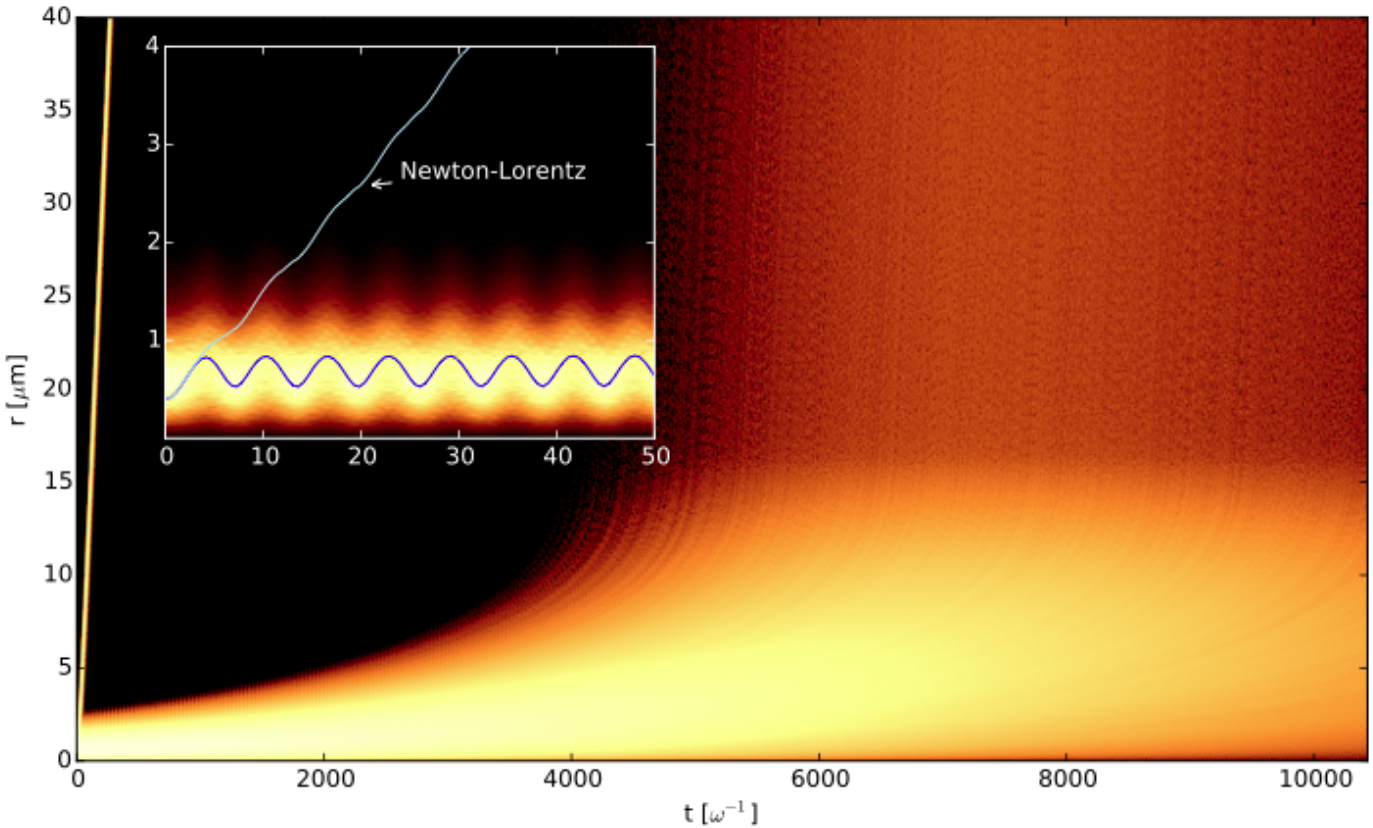

The plot shows the probability density of trapped electrons in a rotating em-field with $a_0 = 800$ as a function of time t and radius r measured from the center of the em-field. As can be seen from the inset the whole ensemble performs an ocillatory guiding center motion and is trapped in the high field region until electrons reach the critical radius $r^* = 17\,\mu$m at $a^* < a_0$.

Radiation friction: PSC simulation

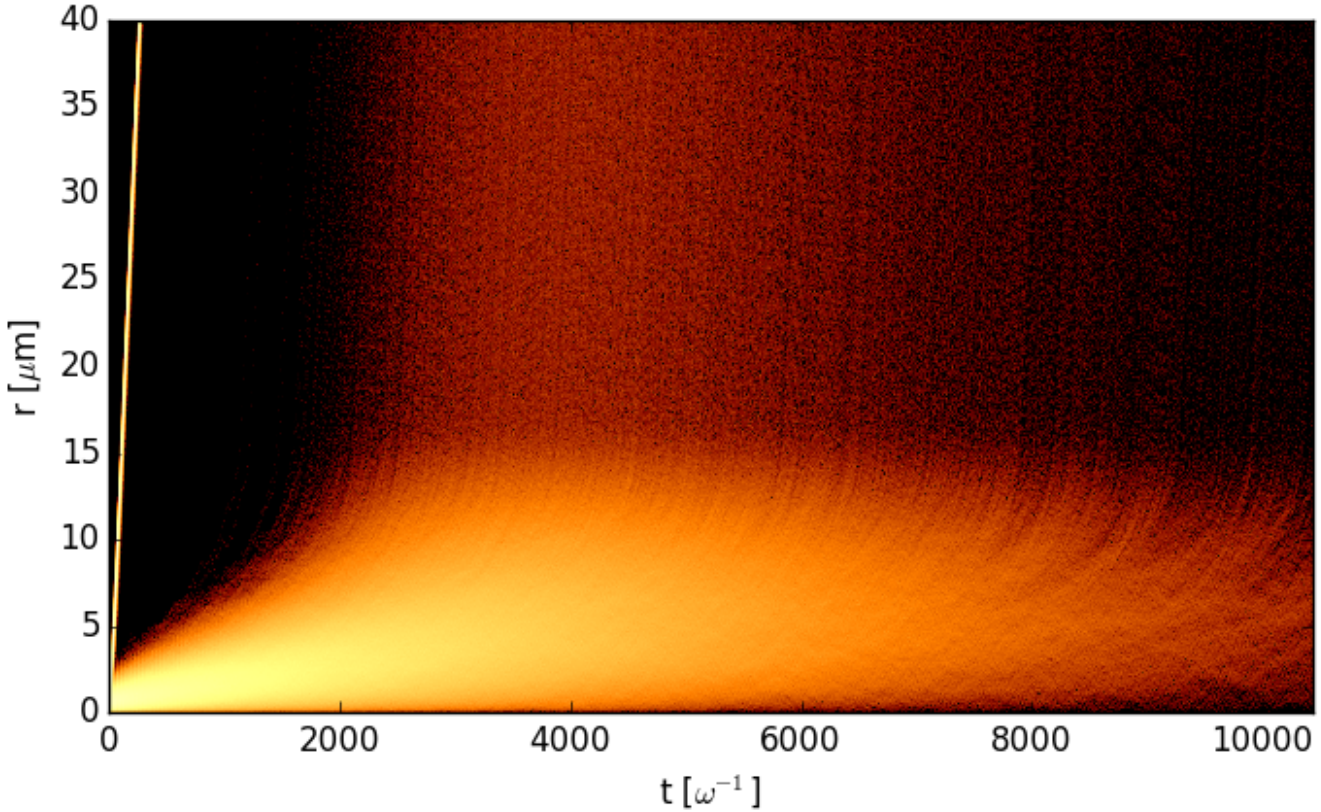

The plot shows the probability density of trapped electrons emitting quantum radiation in the rotating em-field with $a_0 = 800$ as a function of time and radius r measured from the center of the external em-field. Is is seen that electrons emitting quantum radiation exit the high field region faster. The yellow line to the left of the plot shows the path of the electron ensemble without radiation friction.

Radiation friction: PSC simulation

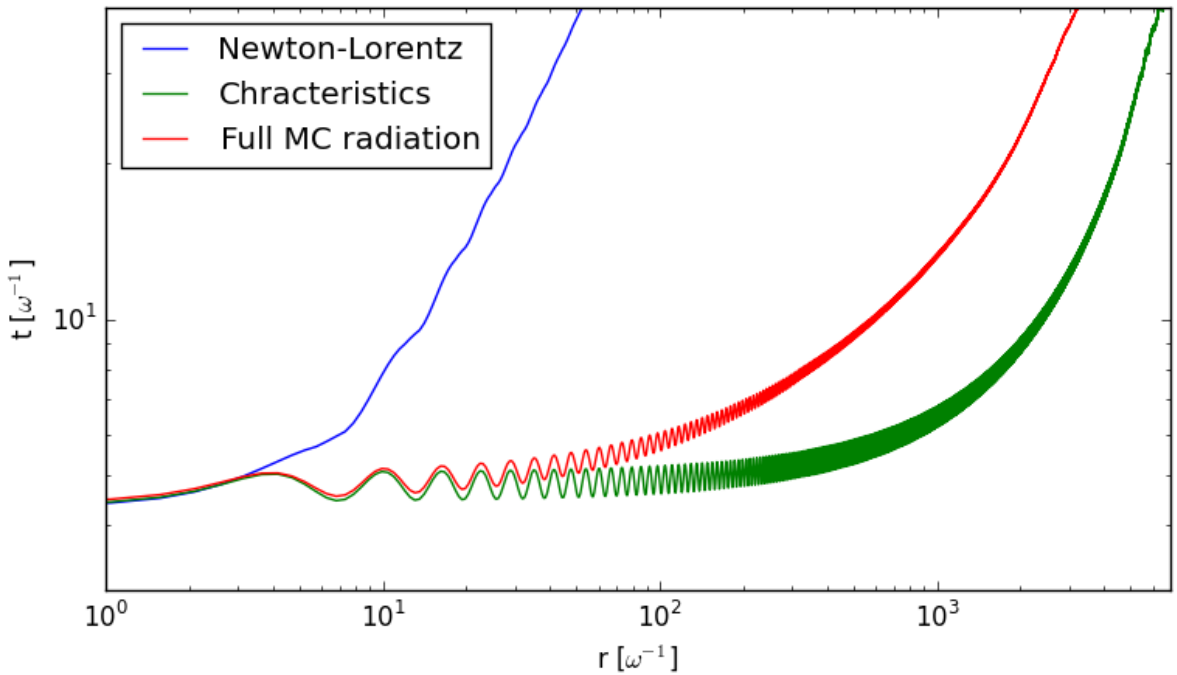

The plot shows the trapping times for the electron probability density for no radiation friction (blue line), classical radiation friction (green line), and quantum radiation friction (red line).

Cascading in an external field: PSC simulation

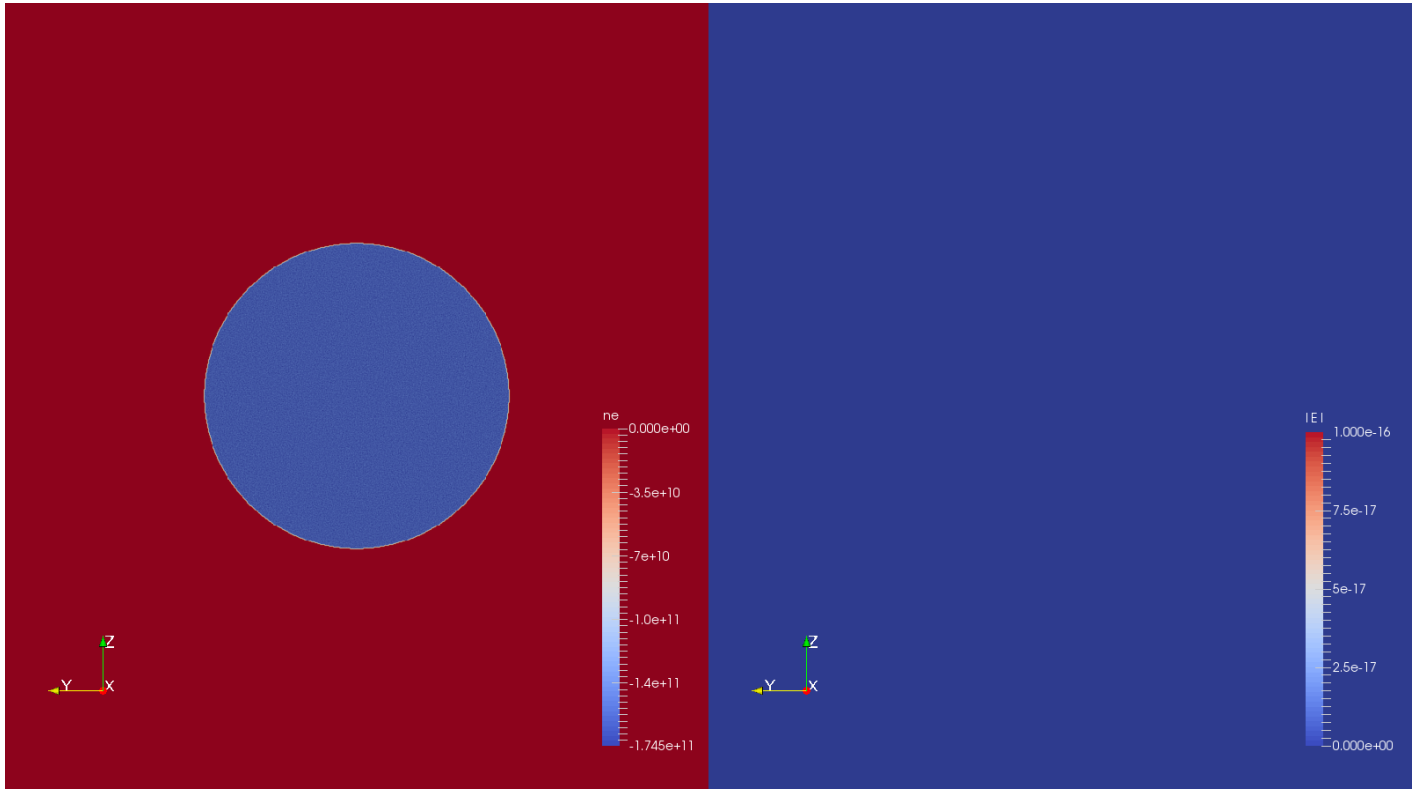

The plot shows the initial electron density of a nano foil and field on the its surface. The initial electron density is $n_e = 1.75 \cdot 10^{11}\,\mathrm{Asm}^{-3}$, while the initial electron number density is $10^{30}\,\mathrm{m}^{-3}$. The diameter of the foil is $90/2\pi\ \mu$m. The laser pulse is Gaussian with a FWHM diameter of $50/2\pi\ \mu$m. The laser pulse hits the foil at the center of the disk.

Cascading in an external field: PSC simulation

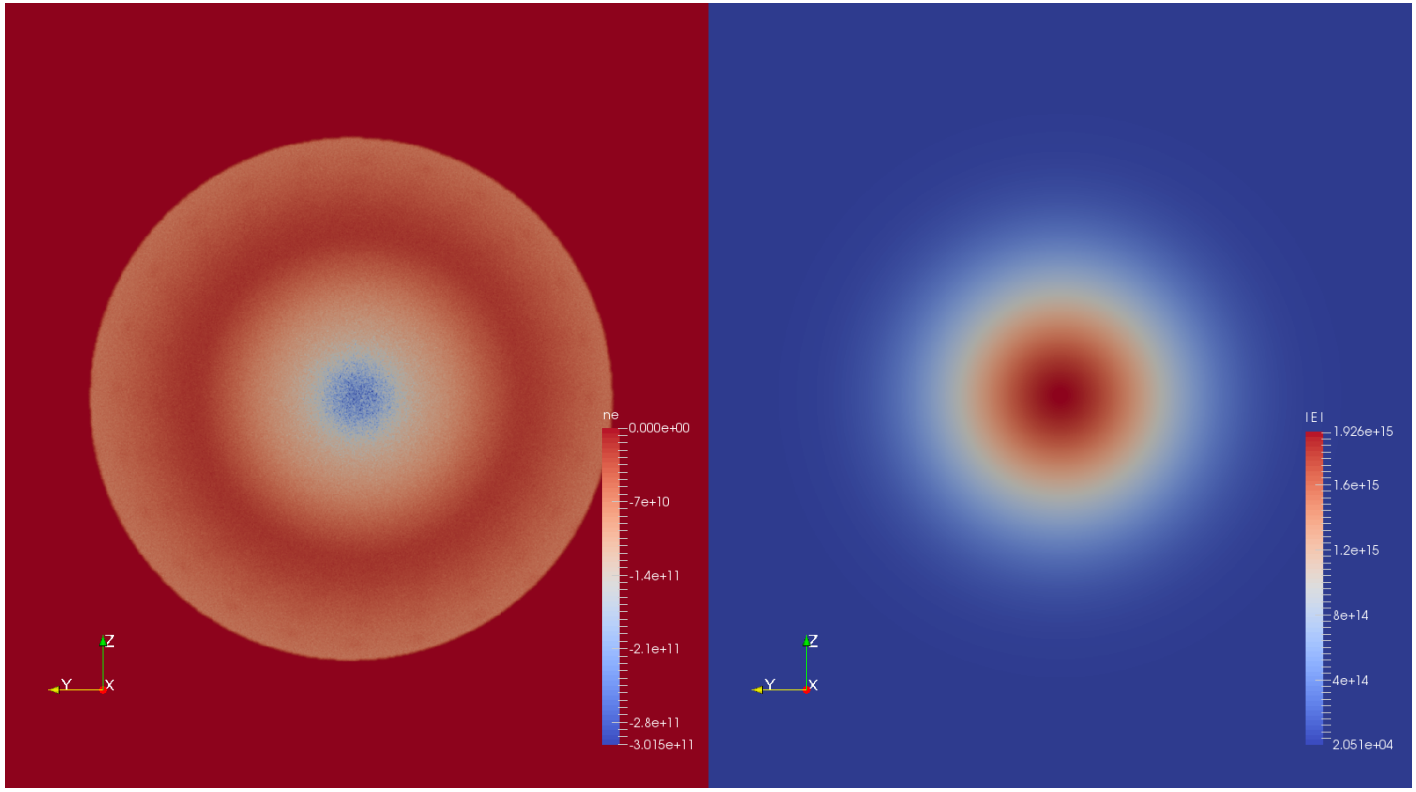

The plot shows the evolution of the electron density during cascading. Two circular counter-propagating laser pulses at $a_0 = 300$ are impinging a low density nano plasma disk. The driving fieldc is considered being an external field. The density grows exponentially. After 400 time steps the electron density is $n_e = 3.08 \cdot 10^{11}\,\mathrm{Asm}^{-3}$. The field strengths of the two laser pulses increase linearly over about 400 time steps up to the peak field.

Cascading in an external field: PSC simulation

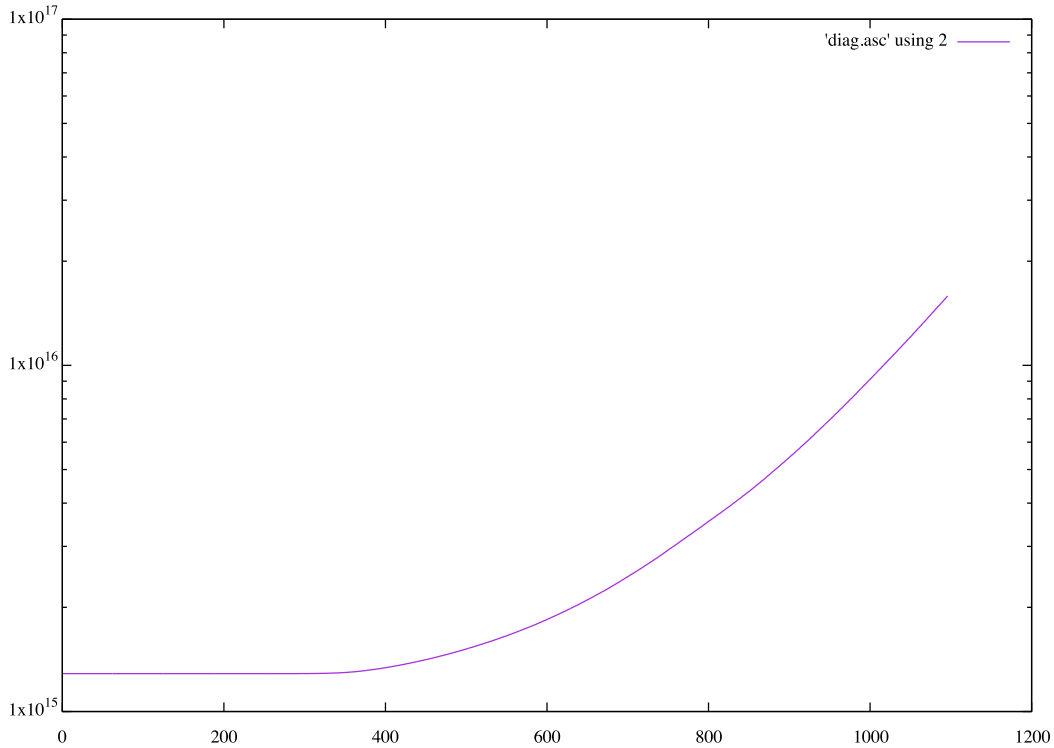

The plot shows the evolution of the electron density of the nano foil. Both laser pulses take about 250 time steps to get to full power. After $n = 1100$ time steps the electron density is $n_e = 2.0 \cdot 10^{16}\mathrm{Asm}^{-3}$. At $n = 1100$ the density is 10^5 over-critical.

Cascading in an external field: The diagnostic

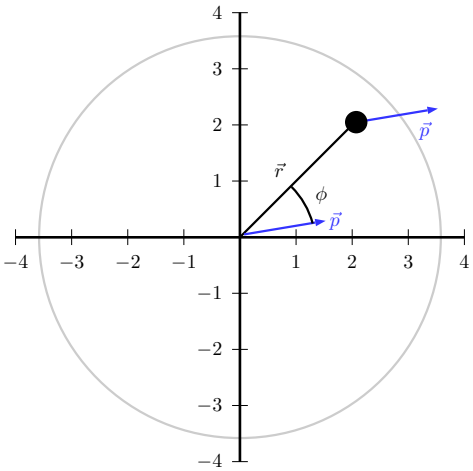

The plot shows the radial position vector $\vec{r}$ of an electron and the momenta $\vec{p}$ of the secondary electron or photon. In the plots shown later the angle ϕ is derived from $|r|\,|p|\,\cos\phi = \vec{r}\cdot\vec{p}$

$$\langle\phi\rangle = \sum_{i=1}^{N_{e,\gamma}(t)} \frac{\vec{r}_i \cdot \vec{p}_i}{|\vec{r}_i||\vec{p}_i|}\,, \tag{23}$$

where the average is over all secondary particles $N_{e,\gamma}(t)$.

Cascading in an external field: PSC simulation

Since the secondary particles will always be emitted parallel to the momentum of the emitting seed particles The angle measure is sensitive to the angular distribution of secondary momenta as a function of position. If secondary particles would exit radially $\langle\phi\rangle$ would be peaked around $\langle\phi\rangle \approx 0$. The average quantum efficiency parameters are given by

$$\langle\chi_{e,\gamma}\rangle = \frac{1}{N_{e,\gamma}(t)} \sum_{i=1}^{N_{e,\gamma}(t)} \chi_{e,\gamma}^{i} \tag{24}$$

Cascading in an external field: PSC simulation

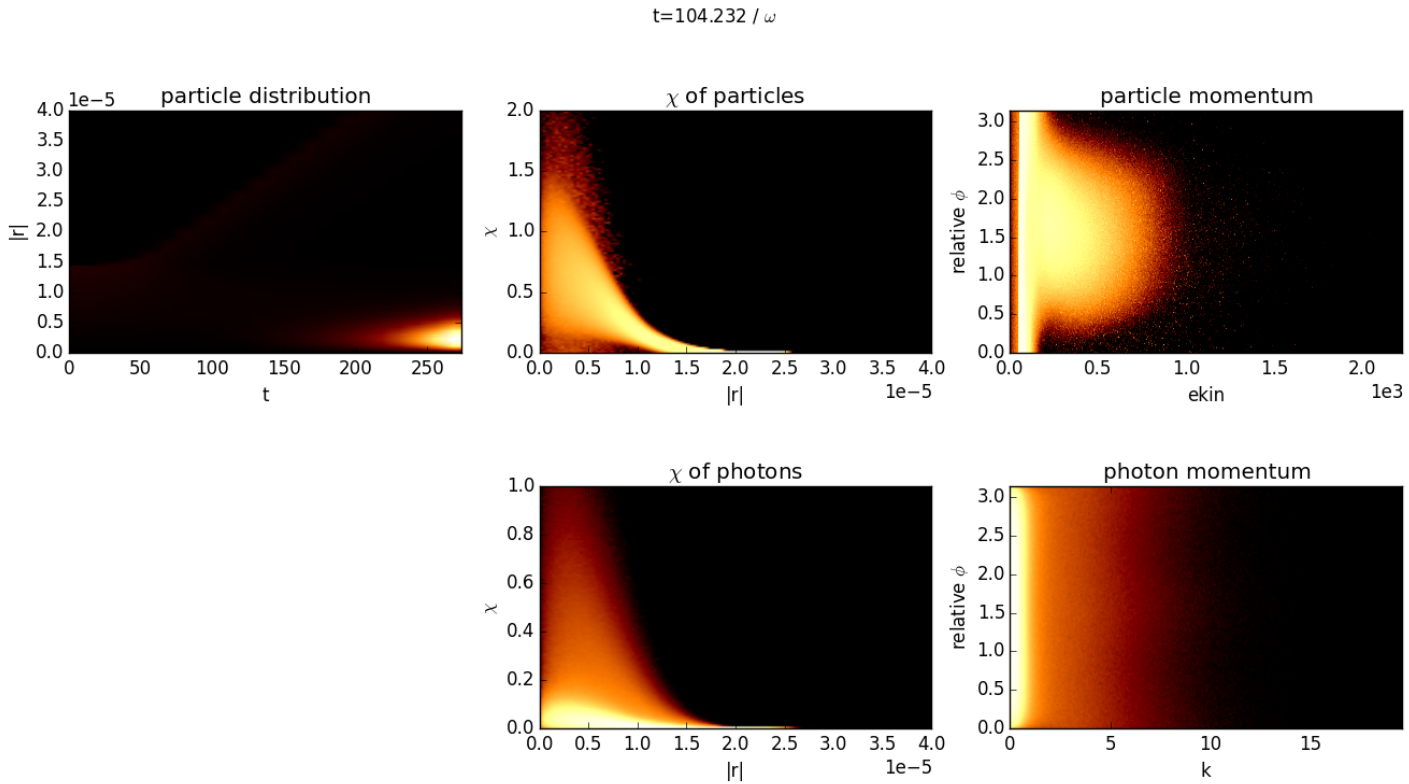

The upper plot to the left shows the radial position of the cascading electrons as a function of time. The second plot on the top shows $\langle \chi_e \rangle$ as a function of radial position. The third plot on the top shows the direction of the cascading electrons as a function of energy. The first plot on the bottom shows $\langle \chi_\gamma \rangle$ as a function of radial position. The second plot on the bottom shows the direction of the photons as a function of k.

Cascading in an external field: PSC simulation

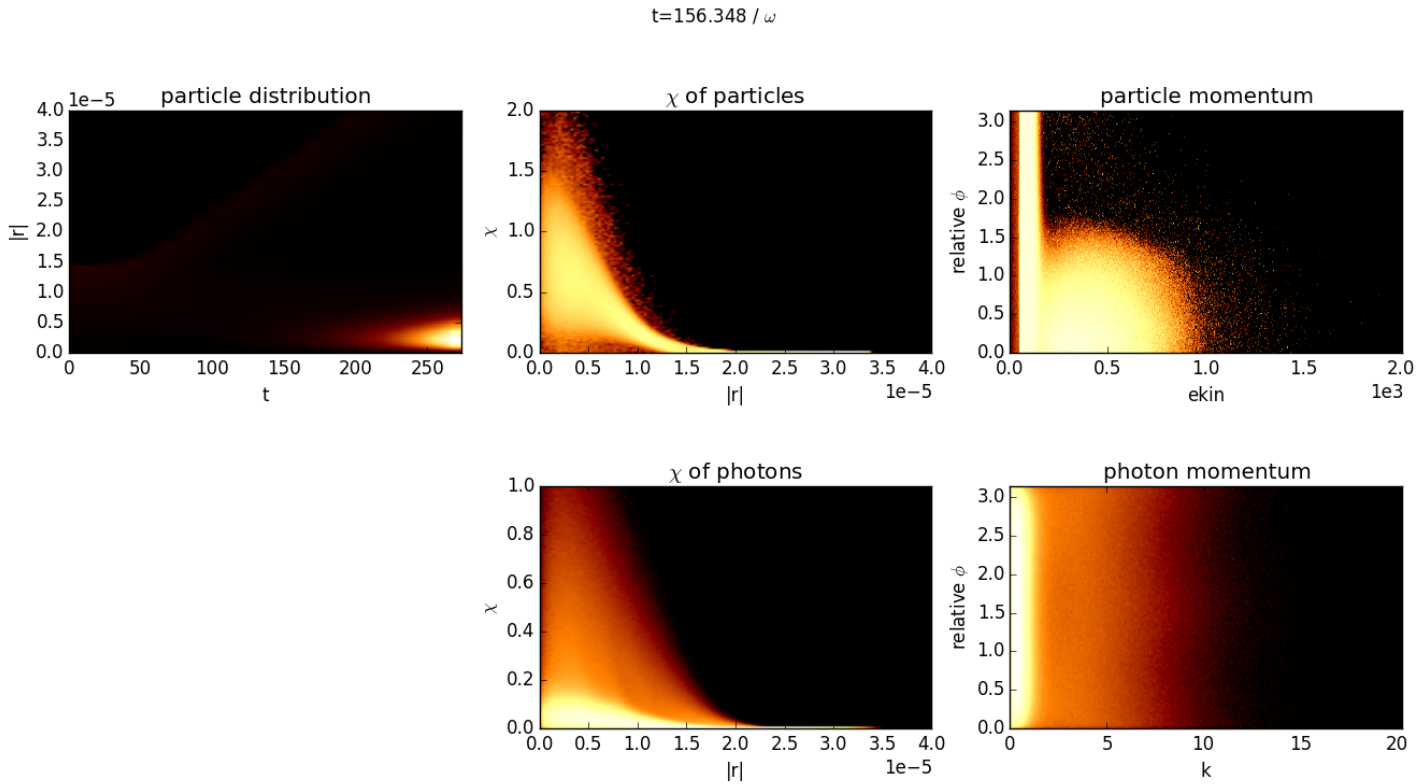

The upper plot to the left shows the radial position of the cascading electrons as a function of time. It shows radiative trapping. The second plot on the top shows $\langle \chi_e \rangle$ as a function of radial position. The third plot on the top shows the direction of the cascading electrons as a function of energy. The first plot on the bottom shows the $\langle \chi_\gamma \rangle$ as a function of radial position. The second plot on the bottom shows the angular distribution of the photons as a function of k.

Cascading in an external field: PSC simulation

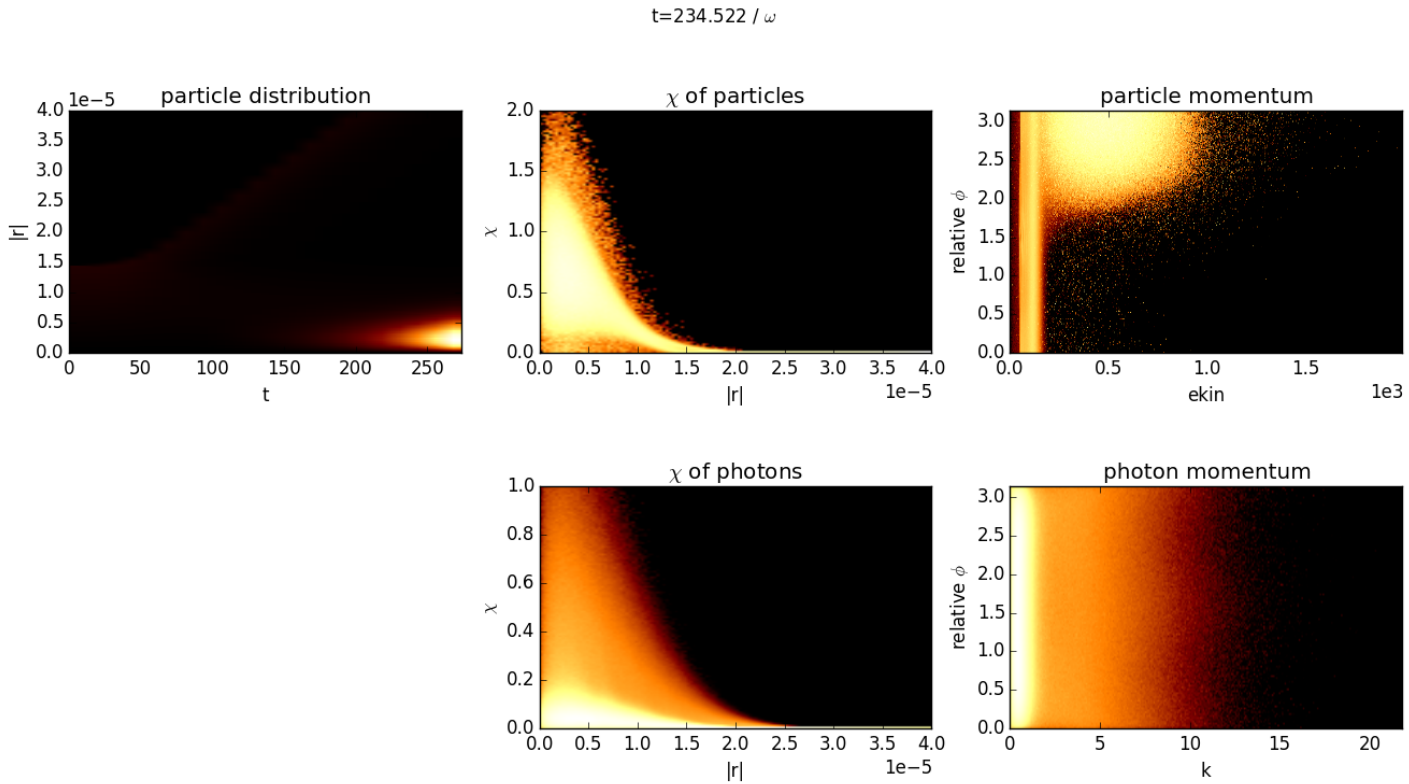

The upper plot to the left shows the radial position of the cascading electrons as a function of time. It shows radiative trapping. The second plot on the top shows $\langle \chi_e \rangle$ as a function of radial position. The third plot on the top shows the direction of the cascading electrons as a function of energy. The first plot on the bottom shows the $\langle \chi_\gamma \rangle$ as a function of radial position. The second plot on the bottom shows the angular distribution of the photons as a function of k.

Cascading in a full field: PSC simulation

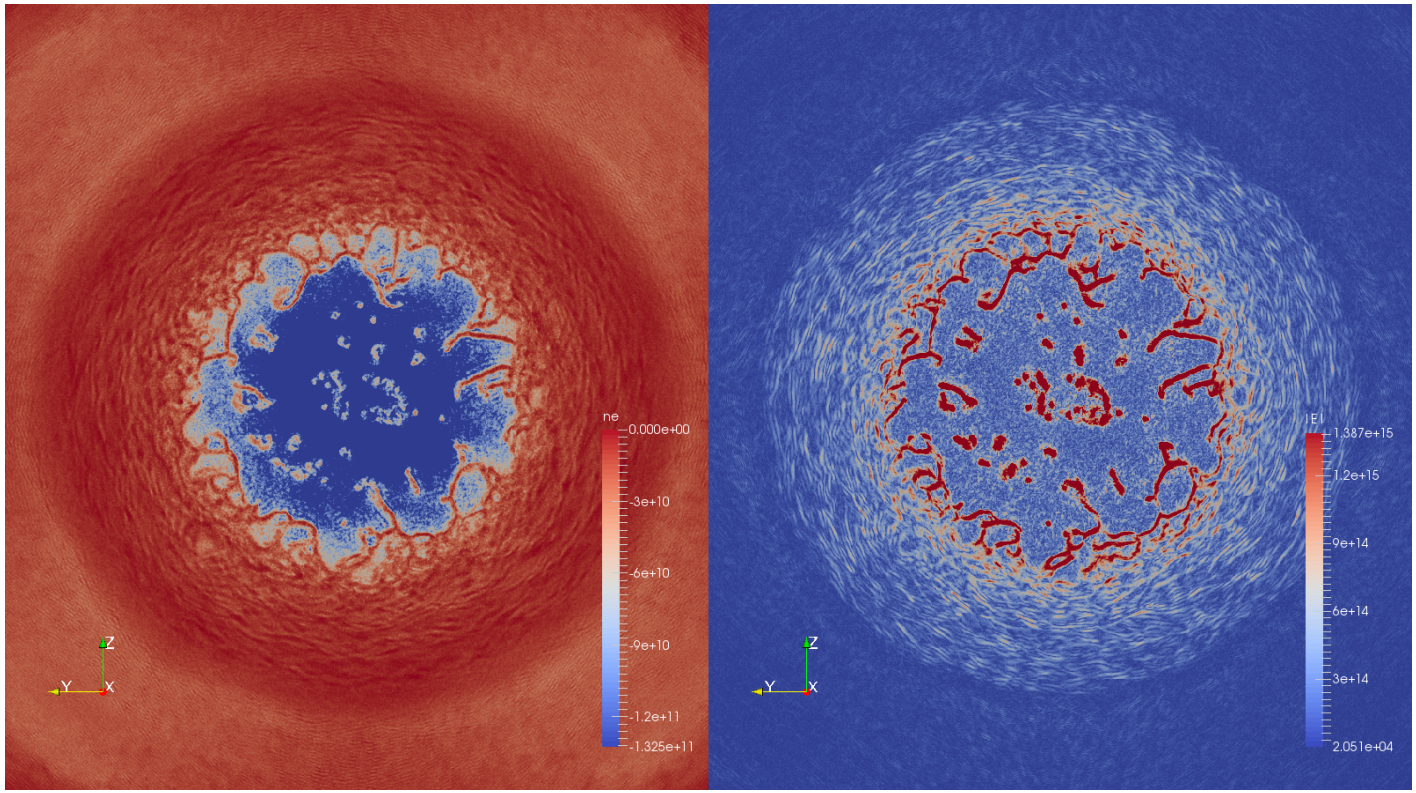

The plot shows the evolution of the electron density during cascading. The simulation starts from two circular counter-propagating laser pulses at $a_0 = 300$ impinging a low density nano plasma disk. The driving field is considered being an external field. The density grows exponentially. The field strengths of the two laser pulses increase linearly up to the peak field.

Cascading in a full field: PSC simulation

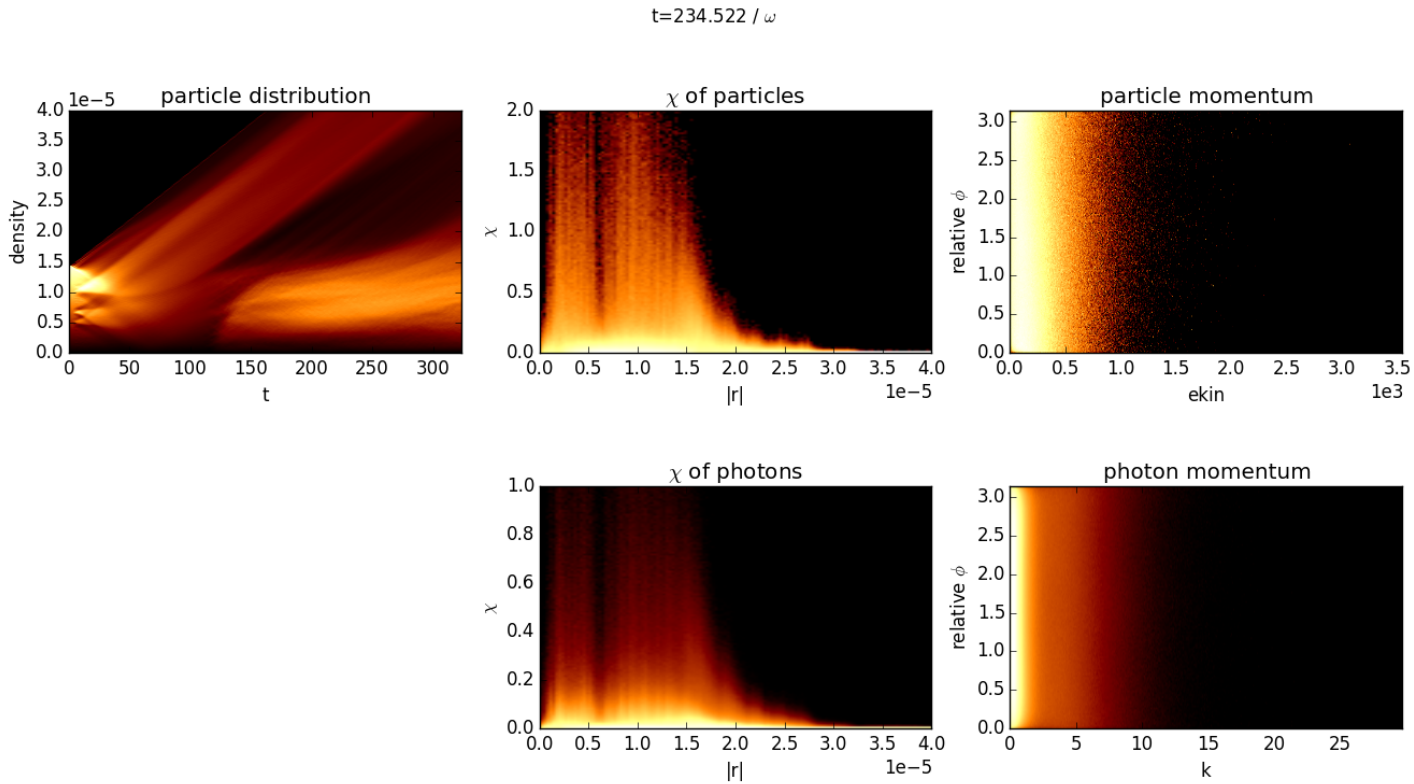

The upper plot to the left shows the radial position of the cascading electrons as a function of time. It shows radiative trapping. The second plot on the top shows $\langle \chi_e \rangle$ as a function of radial position. The third plot on the top shows the direction of the cascading electrons as a function of energy. The first plot on the bottom shows the $\langle \chi_\gamma \rangle$ as a function of radial position. The second plot on the bottom shows the angular distribution of the photons as a function of k.

The Heisenberg-Euler Lagrangian

We define ($\hbar = c = 1$)

$$\mathcal{F} = \frac{F^2}{4E_s^2}\,, \quad \mathcal{G} = -\frac{F\,F^*}{4\,E_s^2}\,, \quad a = \sqrt{\sqrt{\mathcal{F}^2+\mathcal{G}^2}+\mathcal{F}}\,, \quad b = \sqrt{\sqrt{\mathcal{F}^2+\mathcal{G}^2}-\mathcal{F}}\,. \tag{25}$$

We assume

$$\lambda_C \left|\partial_\eta F^{\mu\nu}\right| \ll \left|F^{\mu\nu}\right|\,, \quad \lambda_C = \frac{1}{m}\,. \tag{26}$$

Fields can be considered constant and the effective Heisenberg - Euler Lagrangian in one loop approximation is

$$\mathcal{L}_{HE} = -\frac{m^4}{8\pi^2}\int_0^\infty \frac{ds}{s^3}\,\exp(-s)\left[s^2\,(ab)\,\cot(sa)\,\coth(sb) - 1 + \frac{s^2}{3}\,(a^2-b^2)\right]\,. \tag{27}$$

$\mathcal{L}_{HE}$ disappears for vanishing fields and can have real and imaginary parts. For purely electric fields $\mathcal{L}_{HE}$ has an imaginary part

$$\mathcal{L}_{HE} = -\frac{m^4E^2}{8\pi^2}\int\frac{ds}{s^2}\,\exp\left(-\frac{s}{E}\right)\left(\coth s - \frac{1}{s} + \frac{s}{3}\right) \to Im\mathcal{L}_{HE} \sim \frac{m^4E^2}{8\pi^3}\sum_{n=1}^{\infty}\frac{1}{n^2}\,\exp\left(-\pi\frac{n}{E}\right)\,. \tag{28}$$

W. Heisenberg and H. Euler, Z. Phys. 98, 714 (1936).

Weak field expansion of Heisenberg-Euler

In what follows we consider the weak field expansion of $\mathcal{L}_{HE}$, for which $E \ll 1$ holds. This rules out pair production. We find

$$\mathcal{L}_{HE}^{weak} = -\frac{m^4}{\alpha} \sum_{n=1}^{\infty} \mathcal{L}_n \,, \tag{29}$$

$$\mathcal{L}_1 = \frac{1}{4\pi}\frac{\alpha}{90\pi}\left[\left(\vec{E}^2 - \vec{B}^2\right)^2 + 7\left(\vec{E}\cdot\vec{B}\right)^2\right] \,,$$

$$\mathcal{L}_2 = \frac{1}{4\pi}\frac{\alpha}{315\pi}\left(\vec{E}^2 - \vec{B}^2\right)\left[2\left(\vec{E}^2 - \vec{B}^2\right)^2 + 13\left(\vec{E}\cdot\vec{B}\right)^2\right] \,,$$

$$\mathcal{L}_3 = \frac{1}{4\pi}\frac{4\alpha}{945\pi}\left[3\left(\vec{E}^2 - \vec{B}^2\right)^4 + 22\left(\vec{E}^2 - \vec{B}^2\right)^2\left(\vec{E}\cdot\vec{B}\right)^2 + 19\left(\vec{E}\cdot\vec{B}\right)^4\right]$$

and in addtion we have the Lagrange density for the Maxwell fields

$$\mathcal{L}_{MW} = \frac{m^4}{8\pi}\left(\vec{E}^2 - \vec{B}^2\right) \,, \quad \mathcal{L} = \mathcal{L}_{MW} + \mathcal{L}_{HE}^{weak} \,. \tag{30}$$

The terms $\mathcal{L}_n$ describe effective $2n$ photon scattering. We restrict ourselves to $\mathcal{L}_1$ and $\mathcal{L}_2$.

B. King, P. Böhl, and H. Ruhl, Phys Rev **D**, (2014).

Nonlinear wave equations for $\vec{E}$ and $\vec{B}$

With the help of the Lagrange formalism nonlinear field equations for $\vec{E}$ and $\vec{B}$ are obtained

$$\Box\vec{E} = 4\pi \left[+\vec{\nabla} \times \partial_t \vec{M} + \partial_t^2 \vec{P} - \vec{\nabla}(\vec{\nabla} \cdot \vec{P})\right] , \tag{31}$$

$$\Box\vec{B} = 4\pi \left[-\vec{\nabla} \times \partial_t \vec{P} + \vec{\nabla}^2 \vec{M} - \vec{\nabla}(\vec{\nabla} \cdot \vec{M})\right] , \tag{32}$$

$$\vec{P} = \frac{\alpha}{m^4} \frac{\partial \mathcal{L}_{HE}}{\partial \vec{E}} , \quad \vec{M} = \frac{\alpha}{m^4} \frac{\partial \mathcal{L}_{HE}}{\partial \vec{B}} . \tag{33}$$

We assume that we have a probe field and a strong field

$$F^{\mu\nu} = F_p^{\mu\nu} + F_s^{\mu\nu} . \tag{34}$$

We analyze the equations for the electric field

$$\Box\vec{E} = \vec{T}\left[\vec{E}, \vec{B}\right] , \quad \vec{T}\left[\vec{E}, \vec{B}\right] = 4\pi \left[+\vec{\nabla} \times \partial_t \vec{M} + \partial_t^2 \vec{P} - \vec{\nabla}(\vec{\nabla} \cdot \vec{P})\right] . \tag{35}$$

B. King, P. Böhl, and H. Ruhl, Phys Rev **D**, (2014).

Solution of nonlinear wave equation for $\vec{E}$ in 1D

In what follows probe and strong fields are taken to be of the form

$$\vec{E}_p^0(\phi_p) = \vec{\epsilon}_p\, \mathcal{E}_p\, e^{-\left(\frac{\phi_p}{\Psi_p}\right)^2} \cos\phi_p\,, \quad \vec{E}_s^0(\phi_s) = \vec{\epsilon}_p\, \mathcal{E}_s\, e^{-\left(\frac{\phi_s}{\Psi_s}\right)^2} \cos\phi_s\,, \tag{36}$$

$$\Psi_j = \omega_j \tau_j\,, \quad \phi_j = k_j^\mu x_\mu\,, \quad j = s, p\,, \tag{37}$$

$$\vec{k}_p = (0,0,1)\,, \vec{k}_s = (0,0,-1)\,, \quad \vec{\epsilon}_p \cdot \vec{\epsilon}_p = \vec{\epsilon}_s \cdot \vec{\epsilon}_s = 0\,, \quad \omega_p \tau_s \gg 1\,. \tag{38}$$

Probe and strong fields are counterpropagating plane waves. Initially the total electric field is given by $\vec{E}^0(t,z) = \vec{E}_p^0(x^-) + \vec{E}_s^0(x^+)$, where $x^\pm = t \pm z$ holds. The 1D wave equations is

$$\Box\vec{E} = \vec{T}\left[\vec{E}^0, \vec{B}^0\right]\,, \quad \Box\vec{E}^0 = \Box\vec{B}^0 = 0\,. \tag{39}$$

The solution is given by

$$\vec{E}(t,z) = \vec{E}^0(t,z) + \Delta E(t,z)\,, \tag{40}$$

$$\Delta E(t,z) = \int dt' \int dz'\; G_R(t-t', z-z')\, \vec{T}\left[\vec{E}^0(t',z'), \vec{B}^0(t',z')\right]\,, \tag{41}$$

$$G_R(t,z) = \frac{1}{2}\,\theta(t)\theta(t-|z|)\,. \tag{42}$$

The solution is a sum of scattered forward- and backward-propagating fields as is seen by a partial integration in t'.

B. King, P. Böhl, and H. Ruhl, Phys Rev **D**, (2014).

Iterative solution of wave equation for $\vec{E}$ in 1D

The solution of

$$\left(\partial_t^2 - \partial_z^2\right) \vec{E}^{n+1} = \vec{T}\left[\vec{E}^n, \vec{B}^n\right] \tag{43}$$

is a fixed point after n iteration steps. A graphical representation is:

$$\mathbf{E}_p^{(n+1)} = \mathbf{E}_p^{(0)} + \Delta\mathbf{E}_p^{(n)}$$

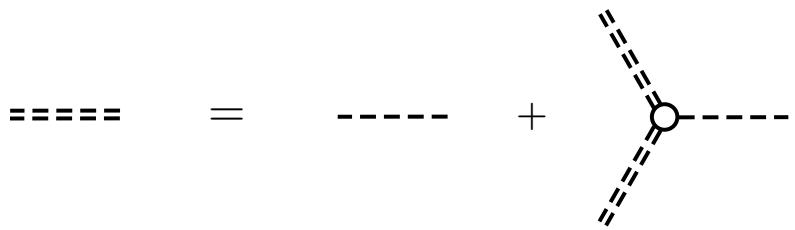

$$\vec{E}^{n+1}(t,z) = \vec{E}^{0}(t,z) + \Delta E^n(t,z)\,, \tag{44}$$

$$\Delta E^n(t,z) = \int dt' \int dz'\; G_R(t-t', z-z')\; \vec{T}\left[\vec{E}^n(t',z'), \vec{B}^n(t',z')\right]\,, \tag{45}$$

$$G_R(t,z) = \frac{1}{2}\,\theta(t)\theta(t-|z|)\,. \tag{46}$$

P. Böhl, H. Ruhl, and B. King, Phys Rev **A 92**, 032115 (2015).

Iterative solution of wave equation for $\vec{E}$ in 1D

It is found that the 1th order solution form 4 photon scattering ($\mathcal{L}_1$ contribution) scales as

$$\Delta E^1 \sim \mu_1 E_s^3 E_p^2 \Phi , \quad \Phi = \omega_p \tau_s . \tag{47}$$

For $\Phi \gg 1$ the perturbation ΔE^1 can become large while the field amplitudes are small. Higher harmonic generation from 4 photon scattering only occurs from the second iteration. It scales as

$$\Delta E_4^2 \sim \mu_1^2 E_s^3 E_p^2 \Phi , \tag{48}$$

while higher harmonic generation from 6 photon scattering occurs from the first iteration. It scales as

$$\Delta E_6^1 \sim \mu_2 E_s^3 E_p^2 \Phi . \tag{49}$$

Since $\mu_1 \ll \mu_2$ is holds that $\Delta E_4^2 \ll \Delta E_6^1$.

P. Böhl, H. Ruhl, and B. King, Phys Rev **A 92**, 032115 (2015).

The numerical scheme

For the 1D geometry given the wave equations can be cast into the form

$$(\mathbf{1}_4 + \mathbf{A})\,\partial_t \vec{f} = (\mathbf{Q} + \mathbf{B})\,\partial_z \vec{f}\,, \tag{50}$$

$$\vec{f} = \begin{pmatrix} E_x \\ E_y \\ B_x \\ B_y \end{pmatrix}, \tag{51}$$

$$\mathbf{Q} = \begin{pmatrix} 0 & 0 & 0 & 1 \\ 0 & 0 & -1 & 0 \\ 0 & -1 & 0 & 0 \\ 1 & 0 & 0 & 0 \end{pmatrix}, \tag{52}$$

$$\mathbf{A} = \frac{m^4}{360\pi^2} \begin{pmatrix} 10B_x^2 - 4B_y^2 + 12E_x^2 + 4E_y^2 & 14B_xB_y + 8E_xE_y & \dots & \dots \\ 14B_xB_y + 8E_xE_y & -4B_x^2 + 10B_y^2 + 4E_x^2 + 12E_y^2 & \dots & \dots \\ 0 & 0 & 0 & 0 \\ 0 & 0 & 0 & 0 \end{pmatrix}, \tag{53}$$

$$\mathbf{B} = \frac{m^4}{360\pi^2} \begin{pmatrix} 8B_yE_x - 14B_xE_y & -14B_xE_x - 20B_yE_y & \dots & \dots \\ 20B_xE_x + 14B_yE_y & 14B_yE_x - 8B_xE_y & \dots & \dots \\ 0 & 0 & 0 & 0 \\ 0 & 0 & 0 & 0 \end{pmatrix} \tag{54}$$

Solved by the PCMOL method.

B. King, P. Böhl, and H. Ruhl, Phys Rev **D**, (2014).

The numerical scheme

We first consider the case $\mathbf{A} = \mathbf{B} = 0$

$$\mathbf{1}_4 \partial_t \vec{f} = \mathbf{Q} \partial_z \vec{f} \,. \tag{55}$$

It is possible to find a transformation $\mathbf{P}$

$$\mathbf{P} = \frac{1}{\sqrt{2}} \begin{pmatrix} -1 & 0 & 0 & 1 \\ 0 & 1 & 1 & 0 \\ 1 & 0 & 0 & 1 \\ 0 & -1 & 1 & 0 \end{pmatrix} \tag{56}$$

such that

$$\mathbf{L} = \mathbf{P}\mathbf{Q}\mathbf{P}^{-1} = \begin{pmatrix} -1 & 0 & 0 & 0 \\ 0 & -1 & 0 & 0 \\ 0 & 0 & 1 & 0 \\ 0 & 0 & 0 & 1 \end{pmatrix}, \quad \vec{u} = \mathbf{P}\vec{f} = \frac{1}{\sqrt{2}} \begin{pmatrix} B_y - E_x \\ E_y + B_x \\ E_x + B_y \\ B_x - E_y \end{pmatrix} \tag{57}$$

such that

$$\partial_t \vec{u} + \mathbf{L} \partial_z \vec{u} = 0 \,. \tag{58}$$

This equation is integrated with an upwind scheme.

B. King, P. Böhl, and H. Ruhl, Phys Rev **D**, (2014).

The numerical scheme

We next consider the case $\mathbf{A} \neq \mathbf{B} \neq 0$. We try to bring the equations into the ODE form

$$\partial_t \vec{u} = \vec{H}(\vec{u}, t) \ , \quad \vec{H}(\vec{u}, t) = -\mathbf{P} \ (\mathbf{1}_4 + \mathbf{A})^{-1} \ (\mathbf{Q} + \mathbf{B}) \, \mathbf{P}^{-1} \, \partial_z \vec{u} \, . \tag{59}$$

We rewrite $\mathbf{A} = \mathbf{MN}$ with

$$\mathbf{M} = \begin{pmatrix} 1 & 0 \\ 0 & 1 \\ 0 & 0 \\ 0 & 0 \end{pmatrix} \ , \quad \mathbf{N} = \begin{pmatrix} a_{11} & a_{12} & a_{13} & a_{14} \\ a_{21} & a_{22} & a_{23} & a_{24} \end{pmatrix} \tag{60}$$

such that

$$(\mathbf{1}_4 + \mathbf{A})^{-1} = \mathbf{1}_4 - \mathbf{M} \ (\mathbf{1}_2 + \mathbf{NM})^{-1} \ \mathbf{N} \, . \tag{61}$$

The inversion of a 4×4-matrix is reduced to the inversion of a 2×2-matrix. The ODE is solved with high precision. The method can be extended to more than 1D with some effort. The simulated system has a length of $320 \, \mu$m and makes use of $2 \cdot 10^5$ stencils in space.

B. King, P. Böhl, and H. Ruhl, Phys Rev **D**, (2014).

The scattered and overlap fields

- The solution consists of an overlap field and a scattered field.
- Scattered and overlap fields can be written as sums over harmonics of the probe field to a good approximation. Details of the analytical calculation will not be presented.
- Scattered and overlap fields depend on the parameters $\mathcal{E}_p$, $\mathcal{E}_s$, $\vec{k}_p$, $\vec{k}_s$, $\vec{\epsilon}_p$, $\vec{\epsilon}_s$, and $\omega_p \tau_s$.

Numerical simulation in 1D of scattered and overlap fields

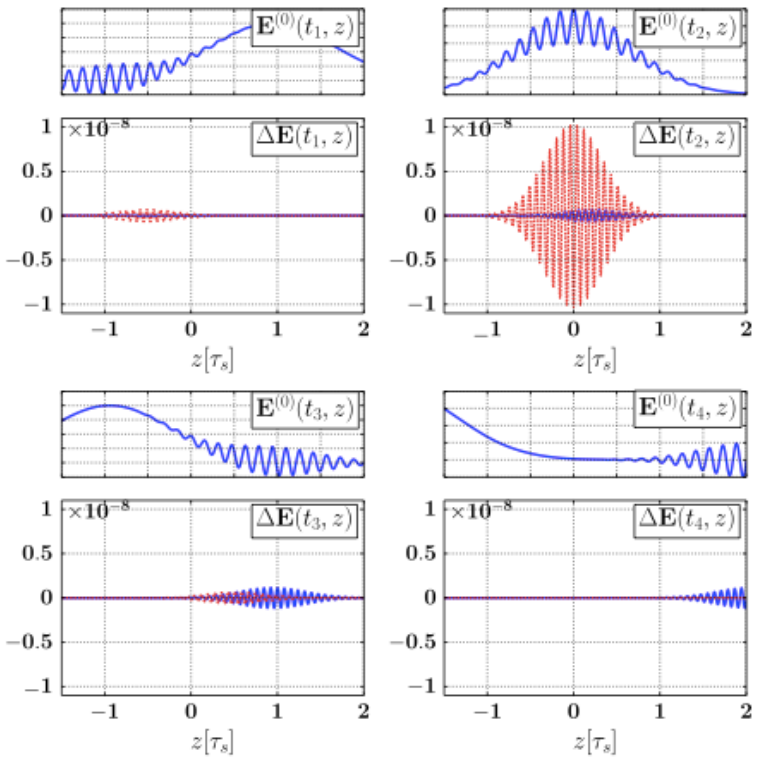

Two plane waves $\vec{E}_p$ and $\vec{E}_s$ interacting, where $\vec{\epsilon}_p \cdot \vec{\epsilon}_s = 0$ and $\omega_p \tau_s \gg 1$. Propagation is along the z-direction, $t_4 > t_3 > t_2 > t_1$, simulation box length 320 μm, resolution $2 \cdot 10^5$ grid points, all fields in probe field units $\mathcal{E}_p$. Small panels show total electric fields of $\vec{E}_p + \vec{E}_s$, larger panels show scattered overlap (red) and asymptotic (blue) 2nd harmonic radiation.

Comparison between theory and numerical simulation in 1D

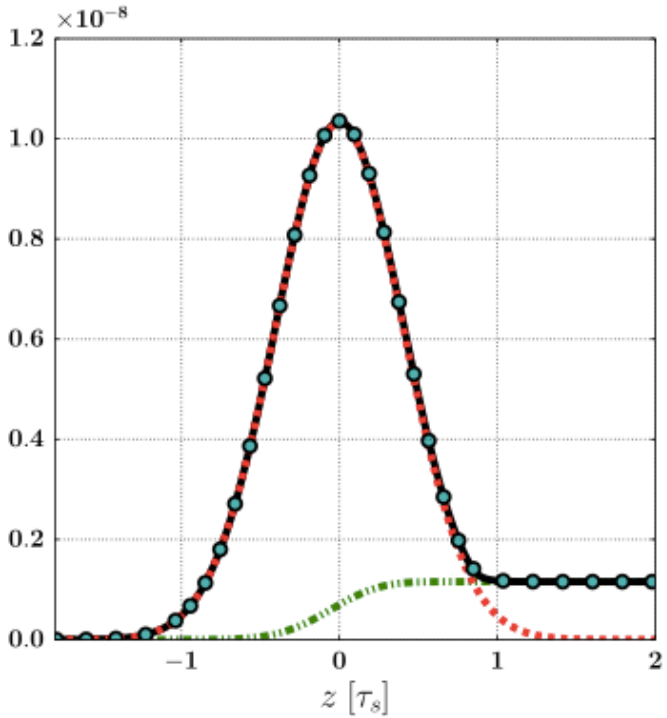

2nd harmonic overlap field (red dashed line) is generated from 4-photon scattering. The asymptotic field (green dashed-dotted line) is generated from 6-photon scattering. There is excellent agreement between simulation (green dots) and theory (solid line). The parameters are $\mathcal{E}_s = 0.02$, $\mathcal{E}_p = 0.005$, $\tau_s = 6.4\lambda_p$, $\tau_p = 5\lambda_p$, and $\omega_p = 0.6$ eV. All fields in units of the Schwinger field.

2D numerical simulation prior to the collision of the pulses

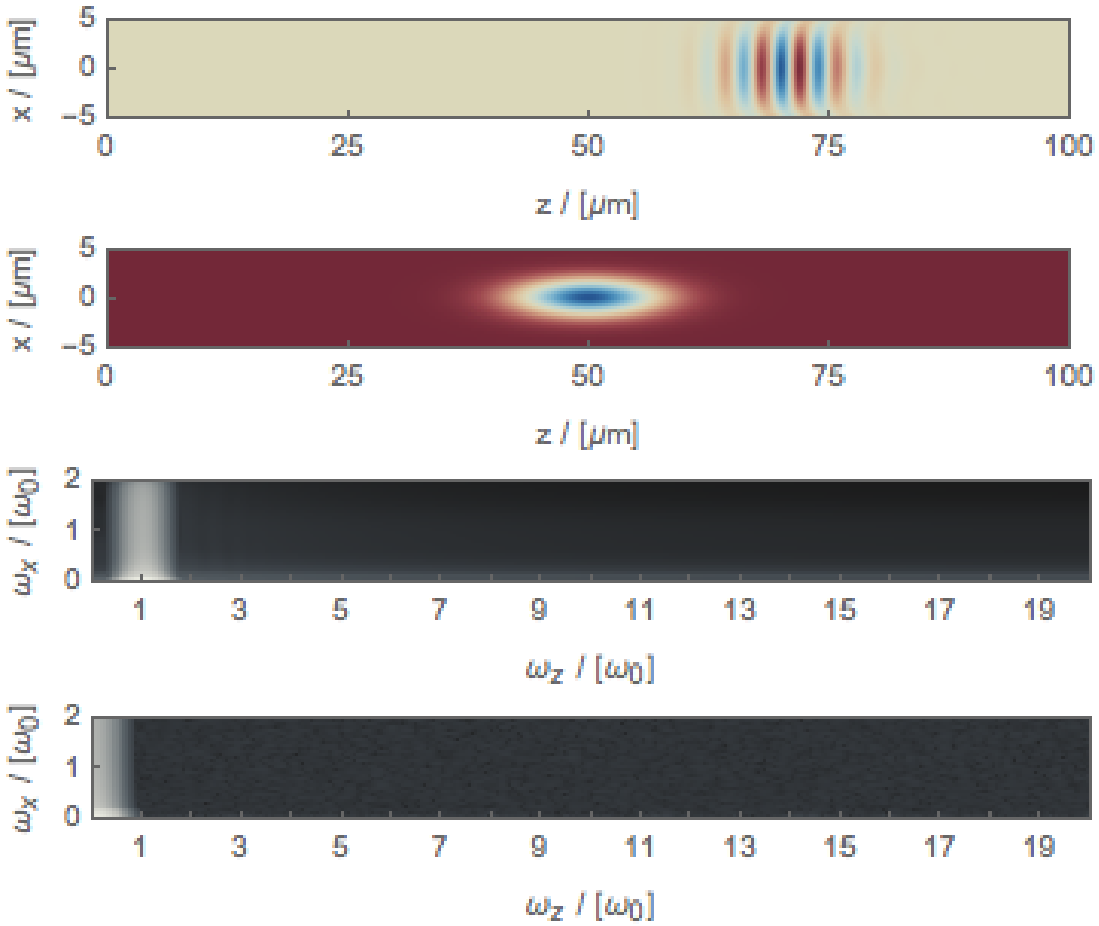

Same parameters as in the 1D case. Top plot: E_x^p. 2nd plot: E_y^s. 3rd plot: Odd harmonics polarized along x. 4th plot: Even harmonics polarized along y.

2D numerical simulation after the collision

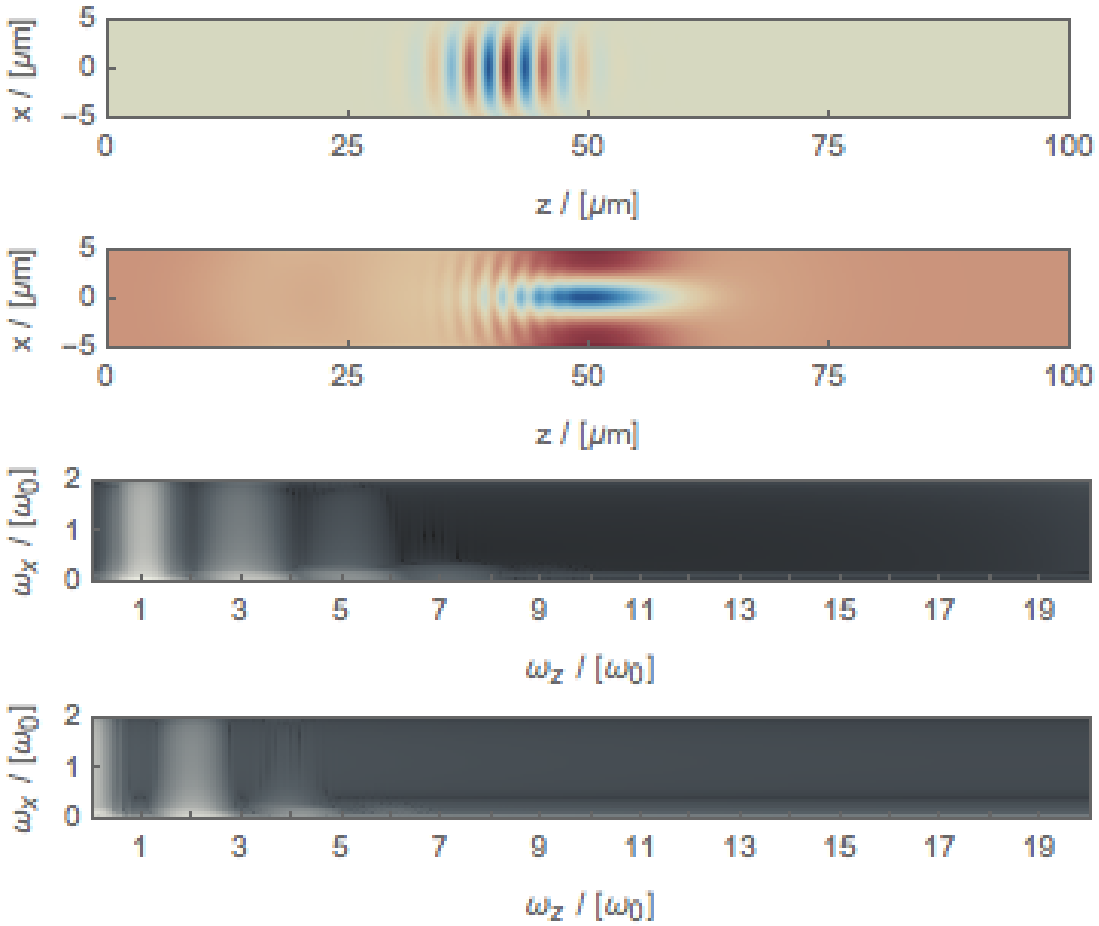

Same parameters as in the 1D case. Top plot: E_x^p. 2nd plot: E_y^s. 3rd plot: Odd harmonics polarized along x. 4th plot: Even harmonics polarized along y. Harmonic emission mostly along the z-direction.

2D numerical simulation after the collision

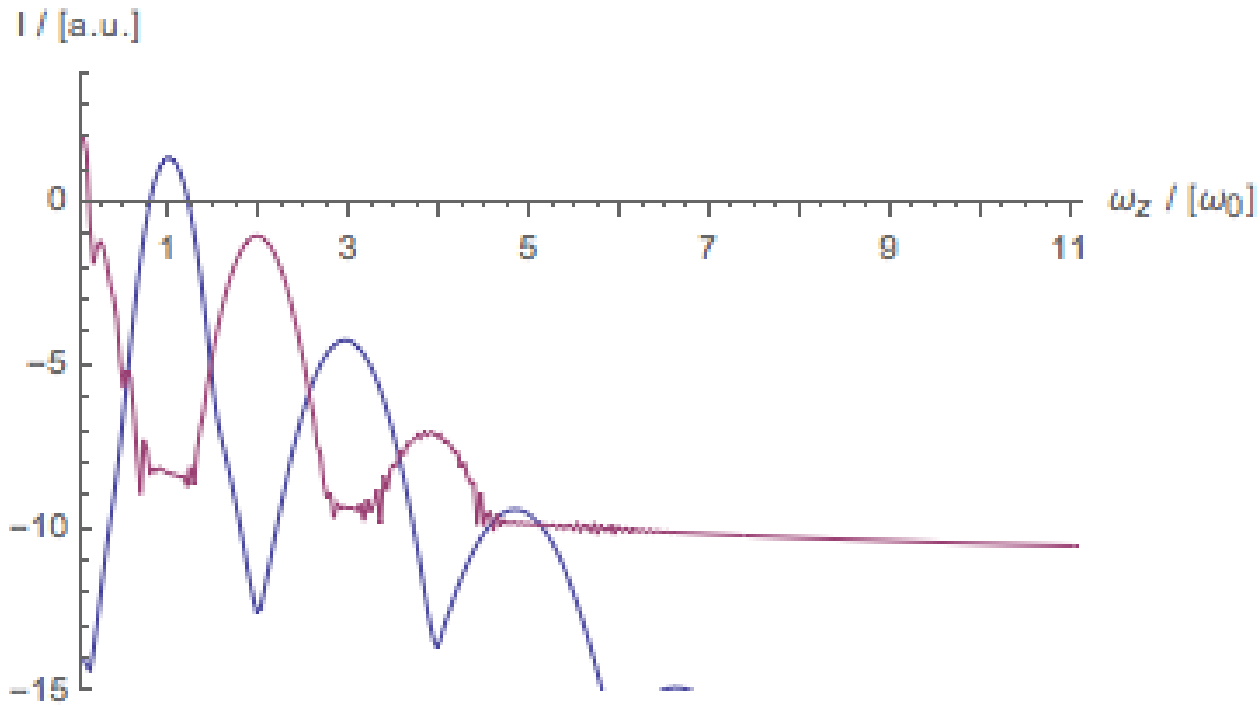

Same parameters as in 1D. Lineout along $\omega_x = 0$, red FFT of E_y, blue FFT of E_x. Polarization of odd harmonics is along the x direction and of even harmonics along the y-direction.

Iterative solution of nonlinear wave equation for $\vec{E}$

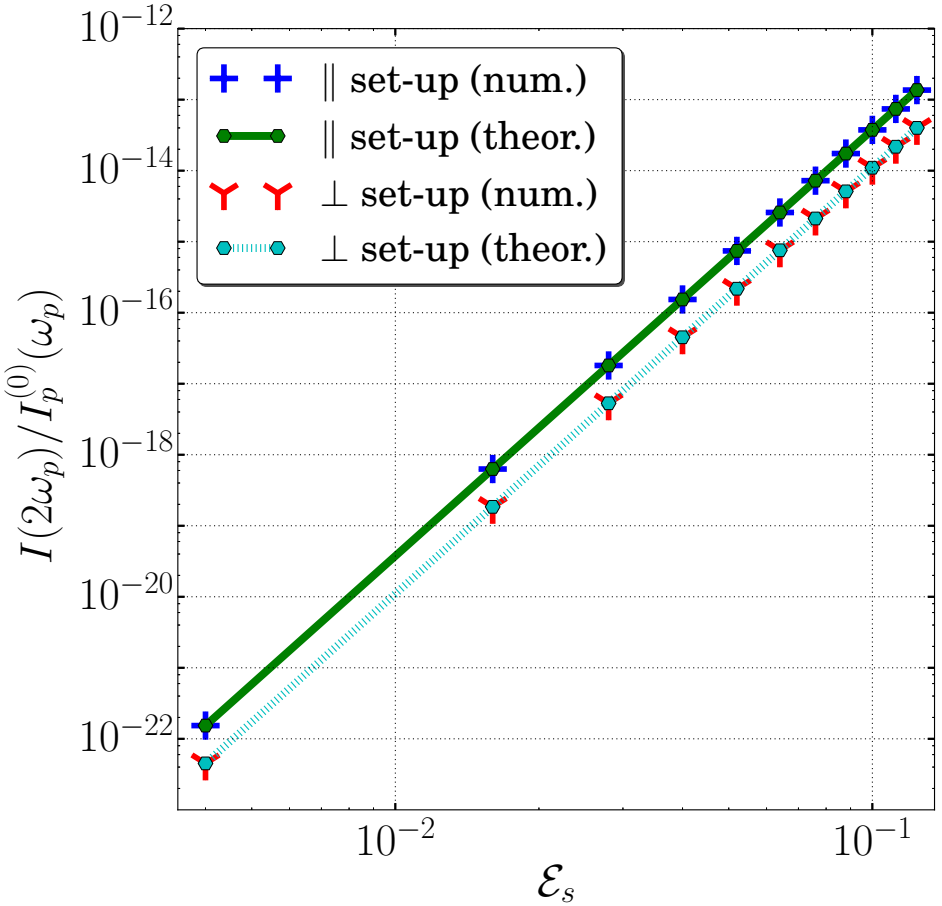

The relative intensity of the second harmonic generated by single six-photon scattering for $\mathcal{E}_p = 10^{-3}$. $\mathcal{E}_{p/s}$ in units of the Schwinger field.

P. Böhl, H. Ruhl, and B. King, Phys Rev **A 92**, 032115 (2015).

Iterative solution of nonlinear wave equation for $\vec{E}$

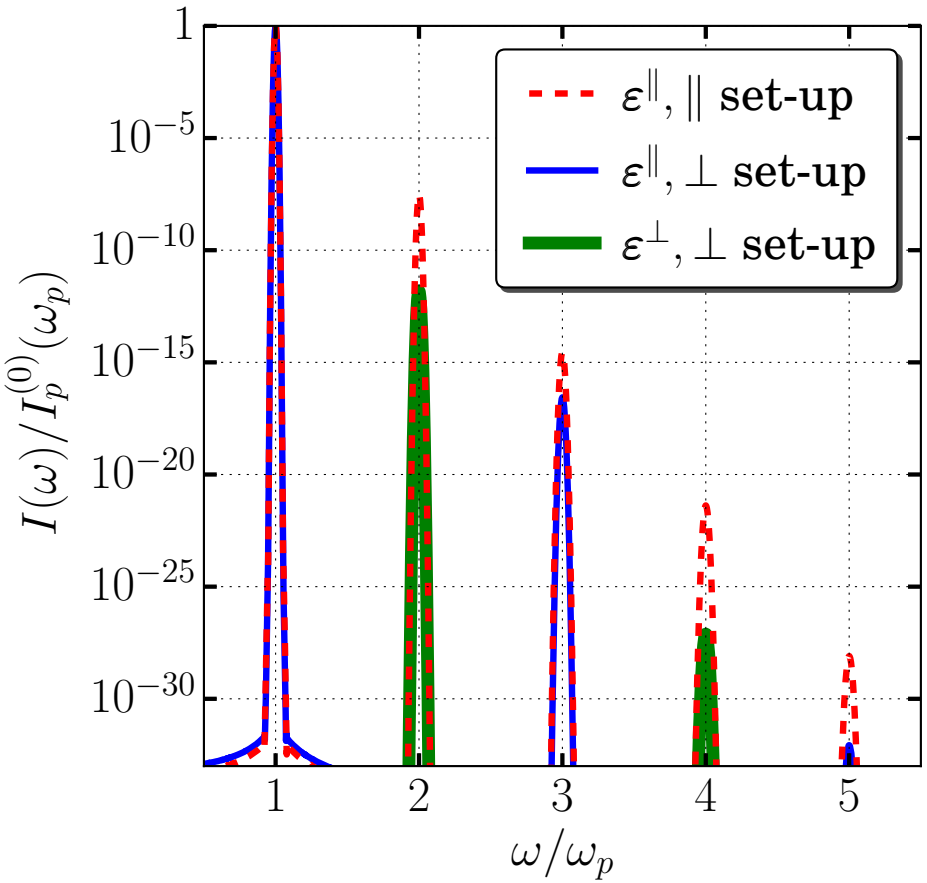

High harmonic generation from multiple four-photon scattering for $\nu_1 = 16\,\mathcal{E}_s^3\mathcal{E}_p\,\Phi = 3.3 \cdot 10^4$.

P. Böhl, H. Ruhl, and B. King, Phys Rev **A 92**, 032115 (2015).

Iterative solution of nonlinear wave equation for $\vec{E}$

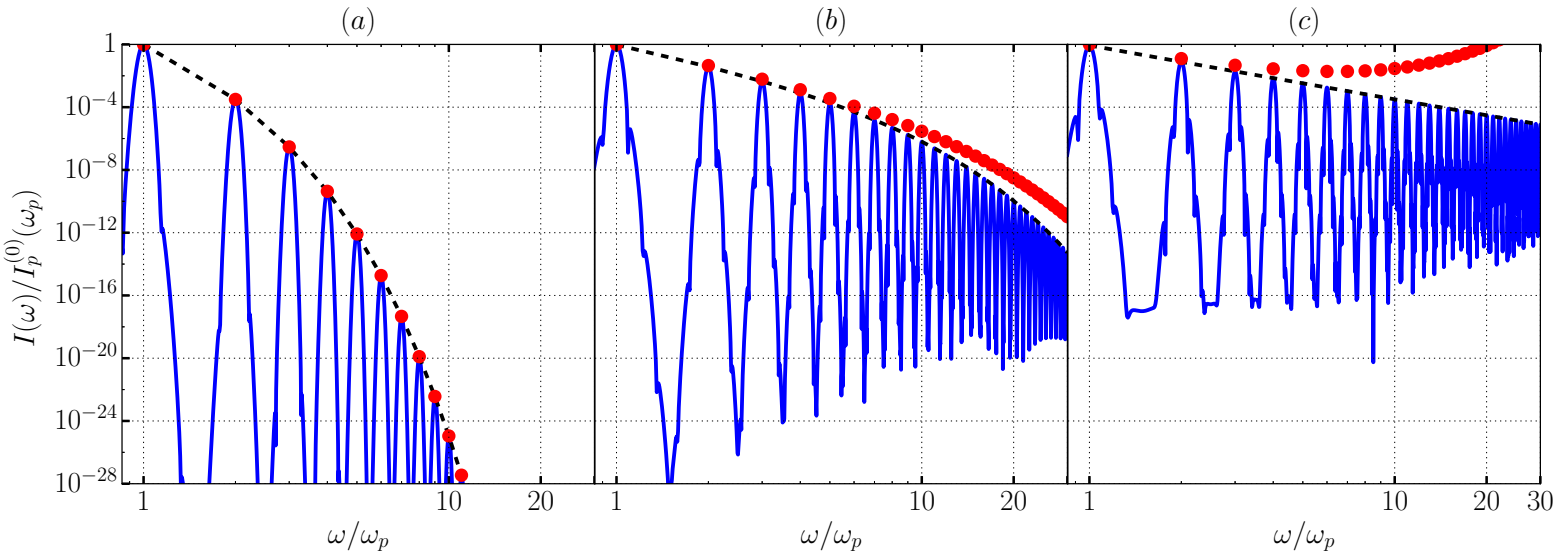

Harmonic spectra in the parallel set-up for different regimes of solution ($\nu_2 = 192\,\mu_2\,\mathcal{E}_s^3$ $\mathcal{E}_s = 0.05, 0.6, 1$). The dots show the leading order perturbative term, the dashed line is the all-order analytical solution and the solid line is from numerical simulation.

P. Böhl, H. Ruhl, and B. King, Phys Rev **A 92**, 032115 (2015).

Summary

- A strong field simulation framework has been discussed.
- The process of radiation friction have been discussed.
- The process of radiation friction and cascading has been discussed.
- General nonlinear wave effects in the vacuum have been discussed.

LMU

References

- **Bamberg K. U.** and **Ruhl H.**, *Extreme Scaling of the PSC on SuperMUC at the LRZ*, inSiDE **12**, 51 (2014).
- Fedotov A., **Elkina N.**, Gelfer E. G., Narozhny N. B. and **Ruhl H.**, *Radiation friction versus ponderomotive effect*, Phys. Rev. A, 90, 053847 (2014).
- **King B.**, **Böhl P.**, and **Ruhl H.**, *Interaction of photons traversing a slowly varying electromagnetic background*, Phys. Rev. **D 90**, 065018 (2014).
- **Elkina N.**, Fedotov A, **Herzing Ch.** and **Ruhl H.**, *Improving the accuracy of simulation of radiation-reaction effects with implicit Runge-Kutta-Nyström methods*, Phys. Rev. E, 89, 053315 (2014).
- **King B.** and **Ruhl H.**, *Trident pair production in a constant crossed field*, Phys. Rev. **D 88**, 013005 (2013).
- **King B.**, **Elkina N.**, **Ruhl H.**, *Photon polarisation in electron-seeded pair-creation cascades*, Phys. Rev. A, 87, 042117 (2013).
- **Elkina N.**, Fedotov A. M., Kostyukov I. Yu., Legov M. V., Narozhny N. B., Nerush E. N. , and **Ruhl H.**, *QED cascades induced by circularly polarized laser fields*, Phys. Rev. ST. Accel. **14**, 054401 (2011).
- Nerush E. N., I. Kostyukov I. Yu., Fedotov A. M., Narozhny N. B., **Elkina N.**, and **Ruhl H.**, *L*aser Field Absorption in Self-Generated Electron-Positron Pair Plasma, Phys. Rev. Lett. **106**, 035001 (2011).
- Legkov M., Fedotov, A., **Elkina N.**, **Ruhl H.**, *2D Monte Carlo simulation of cascades in rotating electric field*, Society of Photo-Optical Instrumentation Engineers (SPIE) Conference Series, Vol. 7994, page 23 (2010).
- Hadad Y., Labun L., Rafelski J., **Elkina N.**, **Klier C.**, and **Ruhl H.**, *Effects of radiation reaction relativistic laser acceleration*, Phy. Rev. D **82**, 096012 (2010).